ER export signals mediate plasma membrane localization of transmembrane protein TMEM72

(膜貫通タンパク質 TMEM72 の細胞膜局在における小胞体輸送シグナルの役割)

申　請　者　　弘前大学大学院医学研究科

脳神経科学領域脳血管病態学教育研究分野

氏　　名　　丁　江麗

指導教授　　今泉　忠淳

Abstract

Transmembrane protein 72 (TMEM72) is involved in normal kidney development and tumorigenesis in renal cell carcinoma. However, the function of TMEM72 has not been experimentally examined; therefore, the role of TMEM72 is incompletely understood. In this study, we initially demonstrated that TMEM72 has four transmembrane domains (TMDs) and a long C-terminal tail. An immunofluorescence analysis showed that TMEM72 is localized on the plasma membrane but not on the outer mitochondrial membrane. Experiments performed with a series of TMEM72 deletion mutants and an evaluation of the unfolded protein response indicated that these TMDs are needed for proper protein folding or assembly. In contrast, domain-specific replacement analysis indicated the essential role of the C-terminal region of TMEM72 in protein transport. Spatial colocalization and immunoprecipitation assays showed that the proximal C-terminal region is responsible for anterograde protein transport. An amino acid sequence analysis and an immunocytochemical evaluation revealed that KRKKRKAAPEVLA, which corresponds to amino acid positions 132-144 in TMEM72, participates in efficient cellular transport. The motifs 132KRKKRK137 and 139APEVLA144 are associated with COPII and are considered to cooperate with membrane trafficking. Because efficient membrane trafficking is crucial for cells to maintain normal function, our data may contribute to elucidating the pathogenesis of membrane trafficking-associated diseases, particularly renal carcinoma and chronic kidney disease.

Introduction

The transmembrane protein (TMEM) family is a group of proteins that integrate with cellular biological membranes [1]. TMEMs act as receptors, transporters, channels, and enzymes and have a variety of key functions in cell transmembrane material transport, energy conversion, signal transduction, and the maintenance of membrane homeostasis [2, 3]. G protein-coupled receptors (GPCRs) are well-known TMEMs [4]. Due to their functions in essential cellular pathways, TMEMs are involved in various diseases, including neurological diseases [5], tumorigenesis [6], and metastatic processes [7]. TMEMs constitute more than 60% of all drug targets [8] and are predicted to be prognostic markers of diseases or tumors [9].

Transmembrane protein 72 (TMEM72) consists of 275 amino acids and has a predicted molecular weight of 37 kDa. The gene encoding TMEM72 is located on human chromosome 10q11.21. Because of its higher expression in ascending limb and distal tubule segments [10], TMEM72 is proposed to be a novel kidney marker [11]. In fetal mice, the *Tmem72* gene is located in the early distal tubules during murine kidney development [12], indicating the involvement of TMEM72 in mammalian kidney development. In contrast, *TMEM72* expression is downregulated in human clear cell renal cell carcinoma (ccRC) [13, 14], and *TMEM72* is considered to be involved in tumor metastasis [6]. Although TMEM72 is thought to exert an essential function in the kidney, its structure, dynamics, and function remain unclear. The function of a protein is often associated with its subcellular localization in organelles [15]. Therefore, clarifying the intracellular distribution of TMEM72 may lead to the elucidation of its function. TMEM72 has been predicted to localize to mitochondria based on its amino acid sequence [16]. Immunohistochemical analysis revealed the granular cytoplasmic and basal membrane distribution of this protein in distal tubule cells [17]. However, no study has experimentally shown the intercellular localization of TMEM72 or presented a molecular characterization of TMEM.

Here, we investigated the subcellular localization of TMEM72. Through peptide deletion, we explored the roles of the transmembrane domains (TMDs) and C-terminal tail of TMEM72 in protein sorting and trafficking. We identified peptides that regulate protein anterograde transport and observed the cooperative effects of multiple ER export signals on the efficient intracellular transport of TMEM72.

Results

Molecular characterization of TMEM72

TMEM72 has been alternatively named kidney-specific secretory protein of 37 kDa. Indeed, we cloned the 828-bp coding region of the *TMEM72* gene from the human embryonic kidney HEK293 cDNA library (Fig. 1A). On the basis of DNA sequence analysis, we further analyzed the TMEM72 amino acid sequence. UniProt (https://www.uniprot.org/) annotation indicated that TMEM72 is a multiple transmembrane protein with four TMDs from amino acid residues 16-36, 41-61, 86-105, and 109-131. We aligned the amino acid sequences of TMEM72 from humans, zebrafish, chicken, chimpanzee, monkey, panda, frog, and alligator and found that the predicted hydrophobic regions have been highly conserved in vertebrates throughout evolution (Fig. 1B). The analysis also showed that TMEM72 has a long hydrophilic domain (residues 132–275) in its C-terminal region.

TMEM72 is located on the plasma membrane

Because TMEM72 has been shown to be expressed in mouse kidney tissue [18], we initially confirmed the expression of TMEM72 in human normal kidney tissue using a rabbit anti-TMEM72 antibody that we generated. The antibody recognizes the C-terminal epitope (residues 241-253) of TMEM72. The distal tubule segments were strongly positive for membrane and cytoplasmic staining. Both the basolateral and apical membranes of the epithelial cells were positively stained. Colocalization analysis showed that TMEM72 partially colocalized with the plasma membrane marker Na+-K+ ATPase (Fig. 2A).

To identify the subcellular localization of TMEM72, we generated 293 cells stably expressing TMEM72. Although we cloned the *TMEM72* gene, TMEM72 protein expression was negligible in parental 293 cells (Fig. 2B). This suggested that the protein expression of TMEM72 is very low in 293 cells. As expected, a sufficient amount of TMEM72 was confirmed in 293 cells stably expressing TMEM72. In TMEM72-expressing cells, TMEM72 was found to localize to the membrane fraction (Fig. 2C). In addition, immunofluorescence analysis showed that TMEM72 colocalized with the plasma membrane marker Na^+-K^+ ATPase (Fig. 2D) [19], indicating the plasma membrane localization of TMEM72. Further microscopic analysis showed the intense localization of TMEM72 at cell–cell junctions (Fig. 2D, arrows) and in pseudopodia (Fig. 2D, arrowheads). In contrast, TMEM72 did not localize to the mitochondrial outer membrane (Fig. 2E). These results indicate that TMEM72 is an integral plasma membrane protein.

Since conserved domain analysis predicted four TMDs in TMEM72, both the N-terminal and C-terminal domains were expected to be exposed to the cytosol or outside the cell. To confirm the directions of the N-terminus and C-terminus of TMEM72, we performed immunofluorescent staining with antibodies recognizing N- or C-terminal epitopes. The N-terminal 3xFLAG tag epitope was recognized by an anti-FLAG antibody. The C-terminal epitope (residues 241-253) was recognized by the rabbit anti-TMEM72 antibody that we generated (Fig. 2B, F). When TMEM72-expressing 293 cells were permeabilized in methanol, the TMEM72 protein was recognized by both anti-3xFLAG (N-terminal) and anti-TMEM72 (C-terminal) antibodies, which were associated with Na^+-K^+ ATPase (Fig. 3A, B). In contrast, neither FLAG nor TMEM72 was detected when cells were not subjected to methanol permeabilization (Fig. 3A, B). These data indicate that both the N-terminal and C-terminal tails of TMEM72 are located on the cytosolic side of the plasma membrane (Fig. 3C).

Depletion of the TMDs results in an unfolded protein response

To investigate the role of the TMDs in the plasma membrane localization of TMEM72, we designed a series of TMD deletion mutants, which are shown in Figure 4A. We observed that the lack of one of the TMDs altered the localization of TMEM72; TMEM72 was not located on the plasma membrane but was found in other organelles (Fig. 4B). TMD1, TMD3, and TMD4 deletion constructs of TMEM72 mainly colocalized with the endoplasmic reticulum (ER) marker calnexin (Fig. 4C). In addition, the TMD2 deletion construct was located in the cytoplasm (Fig. 4C). Because all these mutants were trapped in the first step of the secretory pathway, we next investigated whether TMD depletion activated the integrated stress response (ISR) or unfolded protein response (UPR). The ISR induces the phosphorylation of eukaryotic translation initiatin factor 2α (eIF2α) [20], and the UPR also activates the transcription factor ATF4 [21]. Cells stably expressing the TMD depletion mutants contained phosphorylated eIF2α and nuclear ATF4 (Fig. 4D- G). Upon UPR events, X-box DNA-binding protein-1 (XBP1) mRNA is spliced [22]. Therefore, we further confirmed the role of TMD depletion in the UPR through a quantitative measurement of the spliced form of XBP1 mRNA. We found that the depletion of TMD increased the spliced form of XBP1 mRNA (Fig. 4H), which indicated that the cells were suffering from ER stress. Collectively, these data suggest that the loss of the TMDs leads to misfolding of the protein. Such misfolded proteins are trapped in the ER and unable to be transported to their destination organelle.

The C-terminus of TMEM72 contributes to ER export

Our next goal was to characterize the long C-terminal tail of TMEM72. We used 293 cells stably expressing TMEM72 deletion mutants, as shown in Fig. 5A. Deletion of the C-terminal

domain (ΔC) was further confirmed to drive TMEM72 to localize predominantly to the ER (Fig. 5B, C), while the deletion of all TMDs (ΔTMDs) led to the predominant localization of TMEM72 in the nucleus (Fig. 5B). Since the ΔC construct was still retained in the ER, we carefully interpreted the results to mean that the C-terminal tail may be involved in protein folding or may contribute to ER export or the ER-Golgi-plasma membrane trafficking pathway. Indeed, expression of the ΔC construct did not significantly induce neither the nuclear translocation of ATF4 (Fig. 5D- G) nor the spliced form of XBP1 mRNA (Fig. 5H). These data suggest that the C-terminal domain of TMEM72 is not involved in protein folding or assembly.

To identify whether the C-terminal tail contains ER export signals, we then generated two chimeric proteins, chimeras 115N-72C and 72N-115C, whose C-terminal fragments were replaced with those of TMEM72 and TMEM115, respectively (illustrated in Fig. 6A). TMEM115, a Golgi protein with four TMDs and a long C-terminal tail, is structurally similar to TMEM72 [23]. The C-terminal truncation of TMEM115 (amino acid positions 1-205) was proven to confer an ER retention phenotype, and the C-terminal domain (amino acid positions 206-351) contains a Golgi-targeting signal [23]. As expected, the chimeras 72N-72C and 115N-115C, both of which were reconstituted in cells with TMEM72 and TMEM115, showed cellular distribution patterns similar to those of wild-type TMEM72 and TMEM115, respectively (Fig. 6A, B). The C-terminal truncated form of TMEM115 was retained in the ER [23]. When the TMEM115 C-terminal truncation construct was combined with the C-terminus of TMEM72 (115N-72C), the ER distribution of TMEM115 was absent, and perinuclear localization was observed (Fig. 6B), indicating that the C-terminal ER export signal of TMEM72 could be transferred to the unrelated protein TMEM115. In contrast, chimera 72N-115C showed neither Golgi nor plasma membrane localization (Fig. 6B). It seems that 72N-115C formed an aggregate-like component around the perinuclear region. We observed that the UPR was activated in the 115N-72C and 115N-115C chimeras (Fig. 6C- G). Therefore, we deduced that certain uncharacterized motifs could drive 115N-72C to undergo anterograde transport, although the chimera was unfolded.

Identification of the ER export signal sequence in TMEM72

We next focused on identifying the core signal sequence required for ER export. By sequential truncation analysis of the C-terminal tail, we initially found that deletion of the proximal site of the C-terminal tail reduced the plasma membrane localization of TMEM72 and led to aberrant accumulation in cellular compartments (data not shown). Truncation of amino acid positions 133-275 (Δ133-275 in Fig. 7A) completely abolished the plasma membrane localization of TMEM72, and this mutant was retained in the ER (Fig. 7B). Thus, we speculated

that the proximal region of the C-terminal tail is essential for the ER export of TMEM72. Analyses with a series of truncated forms of the proximal C-terminal tail confirmed that the truncation of codons 132-144 (Δ132-144, KRKKRKAAPEVLA) resulted in substantial retention of the mutant in the ER. In agreement with this result, the localization of a mutant in which the C-terminal tail was deleted (illustrated in Fig. 7A) was reestablished at the plasma membrane upon the addition of KRKKRKAAPEVLA (Fig. 7B, Δ146-275). The levels of ATF4 and the spliced form of XBP1 mRNA were unaltered by these mutants (Fig. 7C- G), suggesting the unrelated role of amino acids 132-144 in the UPR.

Transmembrane proteins are transported through the secretory pathway. The coat protein complex II (COPII) vesicle is a secretory pathway cargo carrier that ferries proteins between ER exit sites and the Golgi [24]. Sec24 specifically binds sorting signals in the cytosolic domains of membrane cargo proteins and usually functions as an obligatory dimeric Sec23/Sec24 protein in selecting cargo molecules for transport to the Golgi apparatus. Therefore, we then hypothesized that TMEM72 is transported from the ER to the Golgi via COPII based on its C-terminal cytosolic tail as a selection signal. We first explored the possible spatial codistribution of TMEM72 and Sec23A. As shown in Fig. 8A, B, 32 h after cotransfection, little TMEM72 was observed on the plasma membrane. In addition, intracellular TMEM72 colocalized with Sec23A. Similar colocalization with Sec23A was partially observed when TMEM72 was deleted at amino acid position 146-275 (Δ146-275 in Fig. 8C, D). In contrast, the truncation of amino acids 133-275 (Δ133-275) decreased the colocalization with Sec 23A (Fig. 8A, B). Notably, TMEM72 was indeed observed on the plasma membrane 48 h after transfection (e.g., Fig. 6B "TMEM72"). Coimmunoprecipitation assays revealed that TMEM72 was pulled down with Sec23A (Fig. 8E, F), and the protein obtained after truncation of 146-275 was still associated with Sec23A (Fig. 8G, H). Collectively, our results indicate that the peptide consisting of amino acids 132-144 (KRKKRKAAPEVLA) may contribute to the COPII-mediated forward trafficking of TMEM72.

The destination of proteins depends on short peptides within individual proteins called *targeting signals* [25]. We found di-hydrophobic motifs (138AA139 and 143VL144) and a consecutive string of the positively charged amino acid peptide sequence 132KRKKRK137 within the putative signal peptide KRKKRKAAPEVLA. Because the hydrophobic motifs were proven to be ER export signals [25], we further examined the role of 132KRKKRKAAPEVLA144 in protein transport. We divided the 132KRKKRKAAPEVLA144 peptide into two halves and generated depletion mutants for each of the two halves, Δ132-137 and Δ139-144, as illustrated in Fig. 9A. The subcellular distributions of wild-type TMEM72,

Δ132-137, and Δ139-144 were demonstrated by immunofluorescence 48 h posttransfection (Fig. 9B, C). Wild-type TMEM72 was predominantly localized in the plasma membrane (72.2%), in both the plasma membrane and ER (21.8%), and in the ER alone (2.4%). In contrast, the deletion of KRKKRK altered the predominant distribution, changing it from a plasma membrane distribution to an ER distribution (59.7%). Additionally, a lower plasma membrane distribution (0.7%) was observed after the deletion of KRKKRK. We noted that the removal of the distal half of the ER export signal peptide (Δ139-144) led to mainly both plasma membrane and ER distribution (Fig. 9C). The levels of ATF4 and the spliced form of XBP1 mRNA were unaltered by these mutants (Fig. 9D- H). These data indicate that the deletion of two halves of the ER export signal results in inefficient anterograde transport but does not activate the UPR.

We performed immunofluorescence and immunoprecipitation assays to further investigate the roles of the two peptides in anterograde export. We initially found that Δ132-137 and Δ139-144 spatially colocalized with Sec23A. Twenty-four hours after transfection, Δ132-137 indeed spatially colocalized with Sec23A (Fig. 10A, B). Neither full-length TMEM72 nor Δ139-144 colocalized with Sec23A after transfection for 24 h (data not shown). Similarly, Sec23A was coimmunoprecipitated with Δ132-137 but not with full-length TMEM72 24 h after transfection (Fig. 10E, F). In contrast, 36 h after transfection, Δ139-144 was also spatially colocalized with Sec23A (Fig. 10C, D). Sec23A was coimmunoprecipitated with either Δ139-144 or full-length TMEM72 (Fig. 10G, H). These data indicate that both 132KRKKRK137 and 139APEVLA144 are important for the packing of TMEM72 into COPII vesicles to regulate ER export.

Discussion

All eukaryotic multispanning membrane proteins are synthesized at the ER and trafficked through the secretory pathway [26]. Export from the ER is the first step in intracellular trafficking. Once correctly folded and fully processed, proteins pass through the ER quality-control system [27]. Improperly assembled proteins are selected for ER retention or degradation [28-30]. In the present study, TMD deletion mutants (ΔTMD1, ΔTMD3, and ΔTMD4), a C-terminal deletion mutant (ΔC), and a membrane-proximal external C-terminal region depletion mutant (Δ132-144) were retained in the ER. Proteins may be retained in the ER due to two types of dysregulation. The first type of dysregulation is a failure in posttranslational processing, such as misfolding or unfolding, or a failure to undergo glycosylation [31], and the other type is ER export signal depletion [32]. The TMD deletion mutants showed nuclear ATF4 translocation and increases in the spliced form of the transcription factor XBP1 mRNA, suggesting that deletion of the TMDs results in protein misfolding or unfolding. However, the C-terminal deletion mutant (ΔC), Δ133-275 and Δ132-144, which lack the whole or partial C-terminal region, did not induce significant translocation of nuclear ATF4 or induction of the spliced form of transcription factor XBP1 mRNA. These data suggest that the sequence in the C-terminal region might not be essential for protein folding or assembly.

Newly synthesized secretory proteins are exported from the ER to the Golgi. A protein that has been modified and then folded in the ER lumen is called cargo [33]. At the ER exit site, the cargo interacts with a carrier protein through the ER export signal sequence in the cargo protein, which is a cytoplasm-oriented peptide [34-36]. Cytoplasmic coat protein complex II (COP II) comprises a set of vesicle coat proteins. The COPII vesicle-mediated ER-Golgi transport of proteins is widely accepted [34]. To date, several cargo-sorting motifs have been shown to engage the COPII vesicle machinery or directly bind COPII [37]. These include the di-acidic sequence (DXE) motif [38-41], di-aromatic and di-hydrophobic motifs [42, 43], and di-aromatic motifs (FF, YY, or FY) [44, 45]. Many cargoes possess multiple signal motifs to mediate efficient anterograde transport. In addition, COPII vesicles recruit a variety of cargoes that do not have common ER export signals [46]. Several ER export signals have been identified in TMEM72: two DXE motifs (164DTE166 and 241DGDSE245) and two di-hydrophobic motifs (138AA139 and 142VL143) in the C-terminal region of TMEM72. However, the sequential truncation of Δ237-275 or Δ161-275 did not alter the plasma membrane localization of TMEM72 (data not shown). These results suggested that these two di-acidic motifs are unrelated to TMEM72 sorting. In contrast, the di-hydrophobic motifs AA and VL are within the ER export signal peptide TMEM72 KRKKRKAAPEVLA (underlined). We found that deletion

of 132KRKKRK137 accelerated the packing of TMEM72 into COP II vesicles and decreased plasma membrane expression. These results indicated the potential role of the KRKKRK peptide in negatively regulating the kinetics of TMEM72 ER export and accelerating subsequent anterograde transport to the plasma membrane. On the other hand, the deletion of 139APEVLA144 did not alter the kinetics of ER export, and the plasma membrane expression level of Δ139-144 was greater than that of Δ132-137. These results suggested that APEVLA peptides may also be involved in the later steps of anterograde transport. The surface composition of channels and receptors can be regulated by controlling their export from the ER [47]. Therefore, the two peptides 132KRKKRK137 and 139APEVLA144 coordinate the ER export and anterograde transport of TMEM72. In contrast, the Δ132-137 and Δ139-144 mutants were partly retained in the secretory pathway. Therefore, we cannot exclude the possibility that the two peptides are also involved in retrograde transport and shuttling between the ER and Golgi via COPII and COPI vesicles. We hope to explore this mechanism in future research.

Twenty-four hours after cotransfection, wild-type TMEM72 was unable to coimmunoprecipitate with Sec23A (Fig. 10E); however, the association was observed 36 h after transfection (Fig. 10G), indicating that full-length TMEM72 had not yet packed into COPII vesicles 24 h after transfection. Immunofluorescence staining also showed that full-length TMEM72 was localized in the ER 24 h after transfection and that localization to the plasma membrane was rarely observed (data not shown). In addition, 36 h after transfection, wild-type TMEM72 was found to be localized outside the ER, such as the plasma membrane, Golgi apparatus, and cytoplasm (data not shown).

Analysis of a stable ΔTMD-expressing cell line showed that the ΔTMD constructs were distributed in the nucleus and cytoplasm (Fig. 4B). After the four TMDs were removed, the ΔTMD constructs could not be sorted to the secretory pathway but were translated by free ribosomes in the cytosol. The ΔTMD proteins were sorted into the nucleus because of the N-terminal “KRKKRK” motif, which was reported to be a nuclear localization signal (NLS) [48]. On the other hand, our data showed that the ΔTMD constructs also showed cytoplasmic localization as well as nuclear localization (Fig. 5B). Although our findings partially explain the role of KRKKRK in TMEM72, further investigation will elucidate the precise mechanism by which the C-terminal region of TMEM72 determines subcellular localization.

Defective protein-membrane trafficking often causes the decreased surface expression of normal functional proteins and the cellular accumulation of aberrant proteins [49]. Loss of expression or

function or toxic overexpression can result in corresponding changes in the associated trafficking pathways, causing observable phenotypes. To date, several diseases have been proven to be associated with defective membrane trafficking. Neurological diseases such as Parkinson's disease (PD) [50], amyotrophic lateral sclerosis (ALS) [51], immunological diseases, and renal diseases [52] are associated with disorders of the secretory pathway. Therefore, TMEM72 may be involved in these diseases.

In summary, we identified the plasma membrane localization of human TMEM72. Four TMDs were found to be essential for protein folding or assembly. TMEM72 can be exported from the ER through COPII vesicles. Finally, two peptides, 132KRKKRK137 and 139APEVLA144, in the C-terminal region are required for COPII cargo selection to coordinate effective anterograde transport. TMEM72 is predicted to be a transporter according to structural and molecular prediction. Our data will help clarify the pathogenesis of renal diseases, including renal cell carcinoma.

Materials and Methods

Cell culture

Human embryonic kidney 293 (HEK293) cells and HeLa cells (Japanese Collection of Research Bioresources Cell Bank, Osaka, Japan) were maintained at 37°C and 5% CO_2, with saturating humidity in Dulbecco's modified Eagle's medium (DMEM) (Sigma–Aldrich, St. Louis, MO) supplemented with 10% fetal bovine serum (FBS) (Perbio Science, Switzerland) and antibiotics (Thermo Fisher Scientific, Carlsbad, CA).

Plasmid construction

The coding region of the *TMEM72* gene was amplified from cDNA isolated from HEK293 cells using KOD plus Neo DNA polymerase (Toyobo, Osaka, Japan) and the specific primers BamHI-TMEM72-F (5'-GACaagcttGCTAGCCCTGGCACCATGCAGCTC-3') and HindIII-TMEM72-R (5'-CCGggatccTCAGAACAGGCCGGTGGC-3'). The products were inserted into the pBluescript SKII (+) cloning vector (pBS-TMEM72) (Thermo Fisher Scientific) and the p3xFLAG-CMV7.1 mammalian expression vector (p3xFLAG-TMEM72) (Sigma–Aldrich). The DNA construct was analyzed by DNA sequencing. To generate stable TMEM72-expressing cells, we initially constructed a pcDNA3.1zeo (+)-3xFLAG expression vector (pcDNA-3xFLAG) by amplification from 3xFLAG to multiple cloning sites of the p3xFLAG-CMV-7.1 vector using the primers NheI-3xFLAG-F (5'-CTGgctagcACCATGGACTACAAAGACCAT-3') and ApaI-3xFLAG-R (5'-AACgggcccACCCGGGATCCTCTAGAGTC-3'). The full-length *TMEM72* gene was cut from p3xFLAG-TMEM72 and inserted into pcDNA3.1-3xFLAG (pcDNA-3xFLAG-TMEM72). Subsequently, the NheI/BamHI site of pcDNA-3xFLAG-TMEM72, containing 3xFLAG followed by full-length TMEM72, was transferred into pcDNA5/FRT (Thermo Fischer Scientific).

To generate a series of TMEM72 deletion mutants, the mutated TMEM72 genes were amplified using the following specific primer pairs:

ΔTMD1-F (5'-CAGGGCCAGTTCAAAAGC-3'),

ΔTMD1-R (5'-TTCCAGCCCAGTCCAGAA-3'),

ΔTMD2-F (5'-ATCTGCTTCCAGTGTCAA-3'),

ΔTMD2-R (5'-ATAGAAAGCCAGGCTTTTGA-3'),

ΔTMD3-F (5'-TTCCTCCACCCGGTCCTG-3'),

ΔTMD3-R (5'-CCAGTGGGCTTTCTCCCT-3'),

ΔTMD4-F (5'-CGGAAGAAGAGGAAAGCT-3'),

ΔTMD4-R (5'-CCAGACCAGGACCGGGTG-3'),

Δ132-137-F (5'-GCTGCCCCCGAGGTGCTGGC-3'),

Δ132-137-R (5'-GCTCAGAAGGAAGTAGGCCA-3'),

Δ139-144-F (5'-TCCCCAGAGCAGTACACAGA-3')

and Δ139-144-R (5'-AGCTTTCCTCTTCTTCCGCT-3').

DpnI was then added and incubated for 1 h at 37°C to cleave the template DNA plasmid.

To generate TMEM72-TMEM115 chimeras, we first amplified the coding region of the *TMEM115* gene by PCR using the specific primers NotI-TMEM115-F (5'-GCTTgcggccgcGATGCAACGTGCCCTGCCA-3') and BamHI-TMEM115-R (5'-CCGggatccTTACAGCGTCGGGGGAGC-3') and inserted the amplicon into p3xFLAG-CMV7.1 (p3xFLAG-TMEM115). Subsequently, using the 3xFLAG-TMEM72 and 3xFLAG-TMEM115 vectors as templates, we amplified the N-terminal TMEMs (115N, residues 1-205 of TMEM115, and 72N, residues 1-131 of TMEM72) and C-terminal TMEMs (115C, residues 206-351 of TMEM115, and 72C, residues 132-275 of TMEM72) that were amplified by PCR. The primers were designed as follows:

NotI-72N-F (5'-GCTTgcggccgcGATGCAGCTCCAGGTGTTC-3'),

BamHI-72N-R (5'-CGCaagcttGCTCAGAAGGAAGTAGGC-3'),

NotI-72C-F (5'-GACaagcttAAGCGGAAGAAGAGGAAAG-3'),

BamHI-72C-R (5'-CCGggatccTCAGAACAGGCCGGTGGC-3'),

NotI-115N- F (5'-GCTTgcggccgcGATGCAACGTGCCCTGCCA-3'),

BamHI-115N-R (5'-CGCaagcttAAGATATACCCAACT-3'),

NotI-115C-F (5'-GACaagcttCGCTTCTACCAGCGCCAT-3')

and BamHI-115C-R (5'-CCGggatccTTACAGCGTCGGGGGAGC-3').

The C-terminal truncated forms of TMEM72 (ΔC, Δ133-275, Δ139-275, and Δ146-275) were generated by PCR using the following primers:

HindIII-TMEM72-F (5'-GACaagcttGCTAGCCCTGGCACCATGCAGCTC-3'),

BamHI-Δ133-275 -R (5'-CCGggatccTCACTTGCTCAGAAGGAAGTA-3'),

BamHI-Δ146-275-R (5'-CCGggatccTCAGGAGGCCAGCACCTCGGG-3')

and BamHI-ΔC-R (5'-CCGggatccTCAGCTCAGAAGGAAGTAG-3').

TMD truncation forms of TMEM72 were generated by PCR using the specific primers HindIII-ΔTMDs-F (5'-GACaagcttAAGCGGAAGAAGAGGAAAGC-3') and

BamHI-ΔTMDs-R (5'-CCGggatccTCAGAACAGGCCGGTGGCT-3').

To generate the Sec23A construct, we first amplified the coding region of the *Sec23a* gene by PCR using the specific primers Xho-Sec23A-F (5'-TCTctcgagGTATGACAACCTATTTGGAA-3') and NotI-Sec23A-R (5'-CCCgcggccgcTCAAGCAGCACTGGACAC-3') and inserted the amplicon into the pCMV-Myc-N vector (pCMV-Myc-Sec23A).

Transient transfection

For immunofluorescence or western blotting, the day before transfection, HeLa cells were seeded in a 12-well plate at a density of 5×10^4 cells per well to obtain a cell density of 50-80% by the day of transfection. Then, the cells were transfected with 800 ng/well plasmid DNA using 1.5 μL of Attractene transfection reagent (QIAGEN, Heidelberg, Germany) for 48 h.

For the coimmunoprecipitation assay, we chose HeLa cells in 100-mm dishes. In addition, 4 μg/well plasmid DNA and 15 μL of Attractene transfection reagent were used for transfection.

Generation of stable cell lines

Cells stably expressing TMEM72 and TMEM72 mutants (ΔTMD1, ΔTMD2, ΔTMD3, ΔTMD4, ΔC, and ΔTMDs) were generated by the Flp-In™ system (Thermo Fisher Scientific) as described previously [53]. Briefly, we cotransfected pcDNA 5/FRT-based constructs and pOG44-expressing Flp recombinase (pcDNA5/FRT: pOG44 = 1:9) into host cells to generate cells stably expressing TMEM72 and the desired mutant by selection with hygromycin (50-100 μg/mL).

Antibodies

For the generation of C-terminal TMEM72 primary antibodies, rabbits were immunized with synthetic polypeptides comprising residues 241-253 (DGDSEPEETTSDT) (SCRUM Inc., Tokyo, Japan). The antiserum titer was determined by enzyme-linked immunosorbent assay (ELISA). Antisera were purified by immunoaffinity purification by SCRUM Inc., and SDS–PAGE and immunofluorescence validated the identity of the refined antibody.

Other antibodies used in this study were as follows: anti-FLAG M2 (Sigma–Aldrich), anti-calnexin (MBL, Tokyo, Japan), anti-Na^+-K^+-ATPase (D4Y7E) (Cell Signaling Technology, Danvers, MA, USA), anti-α 1 sodium potassium ATPase (Abcam, Cambridge, UK), anti-eIF2α (D3), anti-CREB-2 (C-20), anti-c-Myc (9E10) (Santa Cruz Biotechnology, CA, USA), anti-phospho-eIF2α (Ser51) (Cell Signaling Technology, Danvers, MA, USA), anti-Sec23A (Abcam, Cambridge, UK), anti-heat shock protein 70 (Enzo Life Sciences, Farmingdale, NY, USA), anti-Lamin B1 (Proteintech, Rosemont, IL, USA), and anti-β-actin C11 anti-TOM 20 (Santa Cruz Biotechnology, CA, USA). Horseradish peroxidase (HRP)-conjugated anti-mouse, anti-rabbit, and anti-goat IgG (Cell Signaling Technology, Danvers, MA, USA); Alexa Fluor TM 555 IgG (H+L); and Alexa Fluor TM 488 IgG (H+L) (Thermo Fisher Scientific) were the secondary antibodies used in this study.

Subcellular fractionation

Stable TMEM72-expressing and control HEK 293 cells ($1x10^6$ cells) were collected by trypsinization, centrifuged at 500 × *g* for 5 min at room temperature and then rinsed twice with phosphate-buffered saline (PBS, pH 7.4). Membrane/organelle, cytoplasmic, and nuclear fractions were analyzed using an SF PTS Kit (GL Science, Tokyo, Japan) according to the manufacturer's protocol.

Western blot analysis

Cells in 12-well plates were washed twice with PBS, harvested in ice-cold RIPA buffer (0.15 M NaCl, 1% Triton-X 100, 0.5% sodium deoxycholate, 0.1% SDS, and 50 mM Tris-HCl, pH 8.0) containing 6 × SDS sample buffer (0.375 M Tris pH 6.8, 12% SDS, 60% glycerol, 0.6 M DTT, 0.06% bromophenol blue, and 10% β-mercaptoethanol) and incubated for 5 min on ice. Then, the viscous cell lysis was passed 20 times through a 26-gauge needle attached to a 1-mL syringe to prepare a homogeneous suspension. After centrifugation at 12000 × g and 4°C for 20 min, the supernatant was collected in a fresh tube and denaturalized at 56°C for 20 min. Ten microliters of the lysate was subjected to 12.5% SDS–PAGE. After protein transfer onto a polyvinylidene

fluoride (PVDF) membrane (Merck), the membranes were blocked with 5% skim milk in Tris-buffered saline with Tween-20 (TBS-T) buffer for 1 h at room temperature. Subsequently, the membrane was incubated with the diluted primary antibody at 4°C overnight, followed by incubation with the appropriate HRP-conjugated secondary antibodies at room temperature for 1 h. The immunoreactive bands were visualized by using ImmunoStar chemiluminescence detection reagent (FUJIFILM WAKO, Tokyo, Japan.)

Immunofluorescence assay

The cells were seeded onto glass coverslips precoated with a poly-L-lysine solution (Merck). The cells were fixed with 4% formaldehyde in PBS at room temperature for 15 min after rinsing twice with PBS. The cells were then permeabilized with 100% methanol at -20°C and incubated with primary antibody in 2% BSA-PBS overnight at 4°C. The cells were then incubated with fluorescence-labeled secondary antibody at room temperature for 1 hour. Finally, the coverslips were treated with DAPI (Thermo Fisher Scientific). Immunofluorescence was visualized by laser scanning confocal microscopy (C1si laser microscope, Nikon, Tokyo, Japan).

Tissue immunohistochemistry

Paraffin-embedded tissue microarray slides of human normal tissue (types #AA9, 2.0mm, 60 samples) were purchased from Super Biochips, Seoul, South Korea. The slides contained 2 mm spots of 30 human organ tissue in duplicates from 60 individuals of male and female patients. The slides were processed for double-label immunofluorescence. Deparaffinized sections were incubated overnight at 4°C with a mixture of anti-TMEM72 and monoclonal anti-alpha 1 sodium potassium ATPase antibodies (Abcam, Cambridge, UK). The sections were then rinsed and incubated with anti-rabbit IgG tagged with Alexa Fluor 555 or anti-mouse IgG tagged with Alexa Fluor 488 for 1 h at 37°C. The sections were mounted with Vectashield (Vector Laboratories, Inc., Burlingame, CA, USA) and examined with a confocal microscope (C1si laser microscope). Semiquantitative analysis was performed to evaluate the colocalization of TMEM72 and Na-K ATPase using ImageJ.

Coimmunoprecipitation

Cells were washed twice with ice-cold PBS and harvested in hypotonic lysis buffer (10 mM Tris (pH 7.4), 100 mM NaCl, 1.5 mM $MgCl_2$, and 0.5% NP-40) containing protease inhibitor cocktail (Sigma–Aldrich) at the appropriate time after cotransfection. After 30 min of incubation on ice, the lysates were centrifuged at 20,000 x g for 10 min at 4°C. The supernatants were incubated with anti-DYKDDDDK tag antibody magnetic beads (FUJIFILM WAKO) with rotation for 4 h at 4°C. After washing the beads four times with lysis buffer and one time with

1×FLAG wash buffer [50 mM Tris-HCl (7.4), 150 mM NaCl, 0.05% NP-40], the proteins were eluted with 25 μg of 3×FLAG peptide (Sigma–Aldrich) in 100 μL of 1×FLAG wash buffer.

Quantitative real-time RT–PCR (qRT–PCR)

Total RNA was extracted from the indicated cells using a NucleoSpin RNA kit according to the manufacturer's protocol. Single-strand cDNA was synthesized using 500 ng of total RNA, oligo(dT)$_{12-18}$ primers and M-MLV reverse transcriptase (Thermo Fisher Scientific). qRT–PCR was performed using a Bio-Rad CFX real-time PCR thermocycler and SsoAdvanced Universal SYBY Green SuperMix solution (Bio-Rad, CA, USA). Primer pairs for total XBP1 and spliced XBP1 were designed and experimentally verified in previous studies [54, 55]. The results were normalized to GAPDH and obtained from three independent experiments. The primers used were as follows:

Total XBP1 Forward: 5′ -CCTTGTAGTTGAGAACCAGG-3′

Reverse: 5′ -GAGTCAATACCGCCAGAATCCA-3′

Spliced XBP1 Forward: 5′ TGCTGAGTCCGCAGCAGGTG3′

Reverse: 5′ -GAGTCAATACCGCCAGAATCCA-3′

GAPDH Forward 5′ -GCACCGTCAAGGCTGAGAAC-3′

Reverse: 5′ -ATGGTGGTGAAGACGCCAGT-3′

The thermal cycling parameters were the following: step 1, 95 °C for 30 s; and step 2, 95 °C for 10 s and 58 °C for 30 s. Step 2 was repeated for 44 cycles.

Quantitative analysis and statistical analysis

Semiquantitative analysis was performed to evaluate the colocalization of two proteins using ImageJ software provided by the NIH (Bethesda, MD, USA). The merged images are shown as a colocalized pixel map, an intensity scatter plot, and the calculated values for the Pearson's (PCC) and Mander's (tM1 and tM2) correlation coefficients. The data are represented as the means ± standard deviations. The statistical significance of the differences between two groups was evaluated by Student's t test and one-way ANOVA among three groups. A probability value of less than 0.05 ($P < 0.05$) was considered to indicate statistical significance.

Author Contributions

JD conceptualized the study. JD and TM designed the experiments. YS performed the data analyses. JD and RH generated a series of TMEM72-expressing vectors. SK performed real-time PCR and analyzed data. JD, YM, and KS performed immunoblotting and immunofluorescence experiments. JD and TM wrote the manuscript. TI helped with the data analysis and with editing the manuscript. All authors contributed to the article and approved the submitted version.

Acknowledgments

We are grateful to Ms. Kumiko Munakata at the Hirosaki University Graduate School of Medicine for her excellent support.This work was supported by JSPS KAKENHI (17K10012 to T.M.) and the Kobayashi Foundation (to T.M.).

Data Availability Statement

Raw data were generated at Hirosaki University. Derived data supporting the findings of this study are available from the corresponding author (TM) on request.

References

1. Schmit, K. & Michiels, C. (2018) TMEM Proteins in Cancer: A Review, *Front Pharmacol.* **9**, 1345.
2. Attwood, M. M. & Schioth, H. B. (2021) Characterization of Five Transmembrane Proteins: With Focus on the Tweety, Sideroflexin, and YIP1 Domain Families, *Front Cell Dev Biol.* **9**, 708754.
3. Guna, A. & Hegde, R. S. (2018) Transmembrane Domain Recognition during Membrane Protein Biogenesis and Quality Control, *Curr Biol.* **28**, R498-R511.
4. Latorraca, N. R., Venkatakrishnan, A. J. & Dror, R. O. (2017) GPCR Dynamics: Structures in Motion, *Chem Rev.* **117**, 139-155.
5. Chen, Q., Fang, J., Shen, H., Chen, L., Shi, M., Huang, X., Miao, Z. & Gong, Y. (2021) Roles, molecular mechanisms, and signaling pathways of TMEMs in neurological diseases, *Am J Transl Res.* **13**, 13273-13297.
6. Wrzesinski, T., Szelag, M., Cieslikowski, W. A., Ida, A., Giles, R., Zodro, E., Szumska, J., Pozniak, J., Kwias, Z., Bluyssen, H. A. & Wesoly, J. (2015) Expression of pre-selected TMEMs with predicted ER localization as potential classifiers of ccRCC tumors, *BMC Cancer.* **15**, 518.
7. Koteluk, O., Bielicka, A., Lemanska, Z., Jozwiak, K., Klawiter, W., Mackiewicz, A., Kazimierczak, U. & Kolenda, T. (2021) The Landscape of Transmembrane Protein Family Members in Head and Neck Cancers: Their Biological Role and Diagnostic Utility, *Cancers (Basel).* **13**.
8. Overington, J. P., Al-Lazikani, B. & Hopkins, A. L. (2006) How many drug targets are there?, *Nat Rev Drug Discov.* **5**, 993-6.
9. Entenberg, D., Oktay, M. H., D'Alfonso, T., Ginter, P. S., Robinson, B. D., Xue, X., Rohan, T. E., Sparano, J. A., Jones, J. G. & Condeelis, J. S. (2020) Validation of an Automated Quantitative Digital Pathology Approach for Scoring TMEM, a Prognostic Biomarker for Metastasis, *Cancers (Basel).* **12**.
10. Lindgren, D., Eriksson, P., Krawczyk, K., Nilsson, H., Hansson, J., Veerla, S., Sjolund, J., Hoglund, M., Johansson, M. E. & Axelson, H. (2017) Cell-Type-Specific Gene Programs of the Normal Human Nephron Define Kidney Cancer Subtypes, *Cell Rep.* **20**, 1476-1489.
11. El Amrani, K., Alanis-Lobato, G., Mah, N., Kurtz, A. & Andrade-Navarro, M. A. (2019) Detection of condition-specific marker genes from RNA-seq data with MGFR, *PeerJ.* **7**, e6970.
12. Thiagarajan, R. D., Georgas, K. M., Rumballe, B. A., Lesieur, E., Chiu, H. S., Taylor, D., Tang, D. T., Grimmond, S. M. & Little, M. H. (2011) Identification of anchor genes during kidney development defines ontological relationships, molecular subcompartments and regulatory pathways, *PLoS One.* **6**, e17286.
13. Xu, Y., Kong, D., Li, Z., Qian, L., Li, J. & Zou, C. (2021) Screening and identification of

key biomarkers of papillary renal cell carcinoma by bioinformatic analysis, *PLoS One.* **16**, e0254868.

14. Zhang, F., Wu, P., Wang, Y., Zhang, M., Wang, X., Wang, T., Li, S. & Wei, D. (2020) Identification of significant genes with prognostic influence in clear cell renal cell carcinoma via bioinformatics analysis, *Transl Androl Urol.* **9**, 452-461.

15. Itzhak, D. N., Tyanova, S., Cox, J. & Borner, G. H. (2016) Global, quantitative and dynamic mapping of protein subcellular localization, *Elife.* **5**.

16. Winter, J., Hunter, S., Sim, J. & Crome, P. (2011) Hands-on therapy interventions for upper limb motor dysfunction following stroke, *Cochrane Database Syst Rev*, CD006609.

17. Habuka, M., Fagerberg, L., Hallstrom, B. M., Kampf, C., Edlund, K., Sivertsson, A., Yamamoto, T., Ponten, F., Uhlen, M. & Odeberg, J. (2014) The kidney transcriptome and proteome defined by transcriptomics and antibody-based profiling, *PLoS One.* **9**, e116125.

18. Xing, Y., Yang, W., Liu, G., Cui, X., Meng, H., Zhao, H., Zhao, X., Li, J., Liu, Z., Zhang, M. Q. & Cai, L. (2020) Dynamic Alternative Splicing During Mouse Preimplantation Embryo Development, *Front Bioeng Biotechnol.* **8**, 35.

19. Iliescu, A. & Gros, P. (2014) The intracellular carboxyl terminal domain of Vangl proteins contains plasma membrane targeting signals, *Protein Sci.* **23**, 337-43.

20. Pakos-Zebrucka, K., Koryga, I., Mnich, K., Ljujic, M., Samali, A. & Gorman, A. M. (2016) The integrated stress response, *EMBO Rep.* **17**, 1374-1395.

21. Iurlaro, R. & Munoz-Pinedo, C. (2016) Cell death induced by endoplasmic reticulum stress, *FEBS J.* **283**, 2640-52.

22. Yoshida, H., Matsui, T., Yamamoto, A., Okada, T. & Mori, K. (2001) XBP1 mRNA is induced by ATF6 and spliced by IRE1 in response to ER stress to produce a highly active transcription factor, *Cell.* **107**, 881-91.

23. Ong, Y. S., Tran, T. H., Gounko, N. V. & Hong, W. (2014) TMEM115 is an integral membrane protein of the Golgi complex involved in retrograde transport, *J Cell Sci.* **127**, 2825-39.

24. Kirk, S. J. & Ward, T. H. (2007) COPII under the microscope, *Semin Cell Dev Biol.* **18**, 435-47.

25. Kunze, M. & Berger, J. (2015) The similarity between N-terminal targeting signals for protein import into different organelles and its evolutionary relevance, *Front Physiol.* **6**, 259.

26. Hegde, R. S. & Keenan, R. J. (2021) The mechanisms of integral membrane protein biogenesis, *Nat Rev Mol Cell Biol*.

27. Martinez-Gil, L., Sauri, A., Marti-Renom, M. A. & Mingarro, I. (2011) Membrane protein integration into the endoplasmic reticulum, *FEBS J.* **278**, 3846-58.

28. Li, H. & Sun, S. (2021) Protein Aggregation in the ER: Calm behind the Storm, *Cells.* **10**.

29. Sun, Z. & Brodsky, J. L. (2019) Protein quality control in the secretory pathway, *J Cell Biol.* **218**, 3171-3187.
30. Sun, Z., Guerriero, C. J. & Brodsky, J. L. (2021) Substrate ubiquitination retains misfolded membrane proteins in the endoplasmic reticulum for degradation, *Cell Rep.* **36**, 109717.
31. Sim, H. J., Cho, C., Kim, H. E., Hong, J. Y., Song, E. K., Kwon, K. Y., Jang, D. G., Kim, S. J., Lee, H. S., Lee, C., Kwon, T., Yang, S. & Park, T. J. (2022) Augmented ERAD (ER-associated degradation) activity in chondrocytes is necessary for cartilage development and maintenance, *Sci Adv.* **8**, eabl4222.
32. Kincaid, M. M. & Cooper, A. A. (2007) Misfolded proteins traffic from the endoplasmic reticulum (ER) due to ER export signals, *Mol Biol Cell.* **18**, 455-63.
33. Geva, Y. & Schuldiner, M. (2014) The back and forth of cargo exit from the endoplasmic reticulum, *Curr Biol.* **24**, R130-6.
34. Dancourt, J. & Barlowe, C. (2010) Protein sorting receptors in the early secretory pathway, *Annu Rev Biochem.* **79**, 777-802.
35. Phuyal, S. & Farhan, H. (2021) Want to leave the ER? We offer vesicles, tubules, and tunnels, *J Cell Biol.* **220**.
36. Schekman, R. & Orci, L. (1996) Coat proteins and vesicle budding, *Science.* **271**, 1526-33.
37. McCaughey, J. & Stephens, D. J. (2018) COPII-dependent ER export in animal cells: adaptation and control for diverse cargo, *Histochem Cell Biol.* **150**, 119-131.
38. Ma, D., Zerangue, N., Lin, Y. F., Collins, A., Yu, M., Jan, Y. N. & Jan, L. Y. (2001) Role of ER export signals in controlling surface potassium channel numbers, *Science.* **291**, 316-9.
39. Nishimura, N. & Balch, W. E. (1997) A di-acidic signal required for selective export from the endoplasmic reticulum, *Science.* **277**, 556-8.
40. Robert, J., Clauser, E., Petit, P. X. & Ventura, M. A. (2005) A novel C-terminal motif is necessary for the export of the vasopressin V1b/V3 receptor to the plasma membrane, *J Biol Chem.* **280**, 2300-8.
41. Votsmeier, C. & Gallwitz, D. (2001) An acidic sequence of a putative yeast Golgi membrane protein binds COPII and facilitates ER export, *EMBO J.* **20**, 6742-50.
42. Lyu, L., Wang, B., Xiong, C., Zhang, X., Zhang, X. & Zhang, J. (2017) Selective export of autotaxin from the endoplasmic reticulum, *J Biol Chem.* **292**, 7011-7022.
43. Tanemoto, M., Abe, T. & Ito, S. (2005) PDZ-binding and di-hydrophobic motifs regulate distribution of Kir4.1 channels in renal cells, *J Am Soc Nephrol.* **16**, 2608-14.
44. Dominguez, M., Dejgaard, K., Fullekrug, J., Dahan, S., Fazel, A., Paccaud, J. P., Thomas, D. Y., Bergeron, J. J. & Nilsson, T. (1998) gp25L/emp24/p24 protein family members of the cis-Golgi network bind both COP I and II coatomer, *J Cell Biol.* **140**, 751-65.

45. Fiedler, K., Veit, M., Stamnes, M. A. & Rothman, J. E. (1996) Bimodal interaction of coatomer with the p24 family of putative cargo receptors, *Science.* **273**, 1396-9.
46. Barlowe, C. (2003) Signals for COPII-dependent export from the ER: what's the ticket out?, *Trends Cell Biol.* **13**, 295-300.
47. Ma, D. & Jan, L. Y. (2002) ER transport signals and trafficking of potassium channels and receptors, *Curr Opin Neurobiol.* **12**, 287-92.
48. Zhou, J., Doorbar, J., Sun, X. Y., Crawford, L. V., McLean, C. S. & Frazer, I. H. (1991) Identification of the nuclear localization signal of human papillomavirus type 16 L1 protein, *Virology.* **185**, 625-32.
49. Yarwood, R., Hellicar, J., Woodman, P. G. & Lowe, M. (2020) Membrane trafficking in health and disease, *Dis Model Mech.* **13**.
50. Abeliovich, A. & Gitler, A. D. (2016) Defects in trafficking bridge Parkinson's disease pathology and genetics, *Nature.* **539**, 207-216.
51. Hardiman, O., Al-Chalabi, A., Chio, A., Corr, E. M., Logroscino, G., Robberecht, W., Shaw, P. J., Simmons, Z. & van den Berg, L. H. (2017) Amyotrophic lateral sclerosis, *Nat Rev Dis Primers.* **3**, 17071.
52. Lloyd, S. E., Pearce, S. H., Fisher, S. E., Steinmeyer, K., Schwappach, B., Scheinman, S. J., Harding, B., Bolino, A., Devoto, M., Goodyer, P., Rigden, S. P., Wrong, O., Jentsch, T. J., Craig, I. W. & Thakker, R. V. (1996) A common molecular basis for three inherited kidney stone diseases, *Nature.* **379**, 445-9.
53. Dempoya, J., Matsumiya, T., Imaizumi, T., Hayakari, R., Xing, F., Yoshida, H., Okumura, K. & Satoh, K. (2012) Double-stranded RNA induces biphasic STAT1 phosphorylation by both type I interferon (IFN)-dependent and type I IFN-independent pathways, *J Virol.* **86**, 12760-9.
54. van Schadewijk, A., van't Wout, E. F., Stolk, J. & Hiemstra, P. S. (2012) A quantitative method for detection of spliced X-box binding protein-1 (XBP1) mRNA as a measure of endoplasmic reticulum (ER) stress, *Cell Stress Chaperones.* **17**, 275-9.
55. Liu, Z., Xia, Y., Li, B., Xu, H., Wang, C., Liu, Y., Li, Y., Li, C., Gao, N. & Li, L. (2014) Induction of ER stress-mediated apoptosis by ceramide via disruption of ER Ca(2+) homeostasis in human adenoid cystic carcinoma cells, *Cell Biosci.* **4**, 71.

Figure legends

Fig. 1. Characterization of human TMEM72. A. PCR amplification of the TMEM72 coding region. cDNA from HEK 293 cells was amplified by PCR to clone the TMEM72 coding region. The arrow indicates the gene encoding the full-length (FL) coding region of TMEM72. Three independent experiments were performed. B. Multiple sequence alignment of TMEM72 orthologs from 13 species (human (NP_001116848.1), chimpanzee (XP_001154517.2), gelada (XP_025253180.1), mouse (NP_848883.2), dog (XP_025322199.1), frog(XP_040176712.1), zebrafish (NP_001315015.1), bat(XP_024416882.1), fish (XP_026103400.1), alligator (XP_025067259.1), panda (XP_002930538.1), chicken (XP_040531167.1), and pigeon (XP_021144014.1)). Sequences are from the National Center for Biotechnology Information. The sequences highlighted with black indicate the positions with a fully conserved residue. Gray shading indicates less-conserved residues of more than 7 species. Red boxes and green boxes indicate the four predicted hydrophobic regions (transmembrane domains) and the C-terminal tail, respectively.

Fig. 2. Plasma membrane localization of TMEM72. A. A double-labeling immunofluorescence assay of human normal kidney tissue showed the colocalization of TMEM72 (red) and Na+-K+ ATPase alpha (green). B. The protein level of TMEM72 in stable TMEM72-expressing 293 cells was analyzed by western blotting with anti-FLAG, anti-TMEM72 or anti-actin antibodies. C. Stable TMEM72-expressing 293 cells and control cells were harvested and fractionated as described in the "Materials and Methods". The fractionated lysates were subjected to SDS–PAGE. The levels of TMEM72, Na+-K+ ATPase, HSP70, and Lamin B1 were examined using western blotting. D. Stable TMEM72-expressing 293 cells were fixed with 4% paraformaldehyde and costained for FLAG-TMEM72 (red) and Na+-K+ ATPase alpha (green). Arrows indicate cell–cell junctions. Arrowheads indicate cell pseudopodia. Images were captured by confocal scanning microscopy. E. Stable TMEM72-expressing 293 cells were coimmunostained with anti-FLAG (red) and anti-TOM20 (mitochondria) antibodies. F. Coimmunostaining of 293 cells stably expressing TMEM72 with anti-FLAG (red) and anti-TMEM72 (green) antibodies. Scale bars =20 μm. Data are representative of three experiments.

Fig. 3. The N-terminus and C-terminus of TMEM72 are directed toward the cytoplasm. Stable TMEM72-expressing 293 cells were fixed with 4% paraformaldehyde with or without membrane permeabilization. A. FLAG-TMEM72 (red) and Na^+-K^+ ATPse alpha (green) were costained with specific antibodies. Scale bar = 20 μm B. Immunostaining of TMEM72 (red) and Na^+-K^+ ATPase alpha (green) was performed. Scale bar = 20 μm. C. Schematic showing TMEM72 in the plasma membrane. The orange rectangle

represents the FLAG tag at the N-terminus. DGDSEPEETTSDT is the C-terminal epitope (residues 241-253) recognized by the anti-TMEM72 antibody. As shown in Figure 2A and 2B, both terminal ends are thought to reside in the cytoplasm. Data are representative of three experiments.

Fig. 4. Role of the TMEM72 TMDs in the plasma membrane localization of TMEM72. A. Illustration showing the conserved domains of wild-type TMEM72 and the deletion mutants ΔTMD1, ΔTMD2, ΔTMD3, and ΔTMD4, which we designed. All of the TMD-truncated proteins were tagged with FLAG at the N-terminus. B. Coimmunostaining of FLAG (red) and Na+-K+ ATPase (green). Data are representative of three experiments. Scale bar = 20 μm. C. The cells expressing the deletion forms of TMEM72, as shown in Fig. 4A, were coimmunostained with anti-FLAG (red) and anti-calnexin (green) antibodies. Data are representative of three experiments. Scale bar = 20 μm. D. The levels of cytoplasmic ATF4, nuclear ATF4, phosphorylated eIF2α, and total eIF2α expression were evaluated by western blotting using specific antibodies. Data are representative of three experiments. E-G. Quantification of at least three independent WB analyses as in Fig. 4D. H. The levels of both spliced and total XBP1 mRNAs were quantified by qRT–PCR. The relative values for spliced/total XBP1 mRNA (%) were normalized to the control (mock).Three independent experiments were performed. The data are presented as the means ± S.Ds. *P0.05; **P<0.01 (by one-way ANOVA).

Fig. 5. Role of the C-terminal domain A. Illustration showing the conserved domains of the TMEM72 C-terminal truncation (ΔC) and N-terminal truncation (ΔTMDs) forms. The N-termini of both mutant proteins were tagged with FLAG. B. Coimmunostaining of FLAG (red) and Na^+-K^+ ATPase (green). Data are representative of three experiments. Scale bar = 20 μm. C. Coimmunostaining of FLAG (red) and calnexin (green). Data are representative of three experiments. Scale bar = 20 μm. D. The levels of cytoplasmic ATF4, nuclear ATF4, phosphorylated eIF2α, and total eIF2α expression were evaluated by western blotting using specific antibodies. Data are representative of three experiments. E-G, Quantification of at least three independent WB analyses as in Fig. 5D. H. The levels of both spliced and total XBP1 mRNAs were quantified by qRT–PCR. The relative values for spliced/total XBP1 mRNA (%) were normalized to the control (mock). The data are presented as the means ± S.Ds.

Fig. 6. The C-terminus contributes to ER export. A. Schematics showing the conserved domains of TMEM72 and TMEM115 and the TMEM72-TMEM115 chimeras, which we designed. We inserted a Hind III-cleavable site (corresponding to amino acids "KL") in the middle of the chimeras. B. Confocal microscopic images showing HeLa cells transiently

expressing N-terminal FLAG-tagged wild-type TMEM72, TMEM115, and chimeric proteins. The immunofluorescence assay was performed using an anti-FLAG antibody (red). Data are representative of three independent experiments. Scale bar = 20 μm. C. HeLa cells were transiently transfected with vectors expressing chimeras, as shown in Fig. 5A. Forty-eight hours after transfection, the cells were harvested and fractionated as described. Western blotting was performed to evaluate cytoplasmic and nuclear ATF4, nuclear ATF4, phosphorylated eIF2α, and total eIF2α expression. Data are representative of three experiments. D-F. Quantification of at least three independent WB analyses as in Fig. 6C. G. The levels of both spliced and total XBP1 mRNAs were quantified by qRT–PCR. The relative values for spliced/total XBP1 mRNA (%) were normalized to the control (mock). The data are presented as the means ± S.Ds. *P<0.05; **P<0.01 (by one-way ANOVA).

Fig. 7. Identification of the ER export signal sequence within the proximal C-terminal region of TMEM72. A. Illustration showing proximal C-terminal amino acid sequences in TMEM72 and their truncated forms, which we designed. B. HeLa cells were transiently transfected with vectors expressing TMEM72 or its truncated form, as shown in Fig. 7A. Subsequently, the cells were coimmunostained using anti-FLAG (red) and calnexin (green) or Na^+-K^+ ATPase (green) antibodies. Scale bar = 20 μm. Data are representative of three independent experiments. C. HeLa cells were transiently transfected with vectors for the expression of C-terminal truncation mutants, as shown in Fig. 7A. Forty-eight hours after transfection, the cells were harvested and fractionated as described previously. Western blotting was performed to evaluate the cytoplasmic and nuclear ATF4, nuclear ATF4, phosphorylated eIF2α, and total eIF2α expression levels. Data are representative of three independent experiments. D-F. Quantification of at least three independent WB analyses as in Fig. 7C. G. The levels of both spliced and total XBP1 mRNAs were quantified by qRT–PCR. The relative values for spliced/total XBP1 mRNA (%) were normalized to the control (mock). The data are presented as the means ± S.Ds.

Fig. 8. The C-terminus binds COPII to mediate ER export. A. HeLa cells were cotransfected with FLAG-TMEM72 or Δ133-275 and Myc-Sec23 for 32 h. The cells were coimmunostained using anti-FLAG (green) and Sec23A (red) antibodies. Scale bar = 20 μm. Data are representative of three independent experiments. Scale bar = 20 μm. B. Quantification of TMEM72 (n=12) and Δ133-275 (n=10) colocalization with Sec23A from three independent experiments. Each value represents Manders' overlap coefficient (fraction of the total fluorescence signal of Sec23A overlapping with the TMEM signal) obtained from confocal images. The data are presented as the means ± S.Ds. *P<0.05 (by Student's t test); C. HeLa cells were transiently cotransfected with vectors for the

expression of Δ146-275 and Sec23A. Twenty-four hours after transfection, the cells were coimmunostained using anti-FLAG (green) and Sec23A (red) antibodies. Data are representative of three independent experiments. Scale bar = 20 μm. Data are representative of three independent experiments. D. Quantification of Δ146-275 colocalization with Sec23A from three independent experiments. Values represent Manders' overlap coefficient (the fraction of total fluorescence signal of Sec23A overlapping with TMEMs signal), obtained from confocal images. E. HeLa cells were cotransfected with FLAG-TMEM72 and Myc-Sec23A for 32 h. G. HeLa cells were cotransfected with FLAG- Δ146-275 and Myc-Sec23 for 24 h. (E, G). The cells were lysed in hypotonic lysis buffer and subjected to immunoprecipitation with anti-FLAG beads. Coimmunoprecipitation was performed using anti-FLAG magnetic beads, and proteins were analyzed by western blotting. Three independent experiments were performed. F, H. Quantification of the protein level of Co-IP Sec23A/IP FLAG.

Fig. 9. The proximal halves of the ER export signal peptides regulate protein surface expression. A. Illustration showing TMEM72 and a half truncation mutant of the ER export signal peptide. B. HeLa cells were transiently transfected with vectors for the expression of Δ132-137 and Δ139-144, as shown in Fig. 9A. At 48 h posttransfection, cells were coimmunostained using anti-FLAG (red) and calnexin (green) or Na^+-K^+ ATPase (green) antibodies. Subcellular localization patterns are shown as plasma membrane (PM), PM+ER, and ER. Scale bar = 20 μm. C. Based on the subcellular distribution patterns, the wild-type TMEM72 Δ132-137 and Δ139-144 constructs were classified as localized in the PM, ER+PM, or ER, as shown in 9C. The distribution (%) of each pattern was calculated on the basis of 39 images (total 442 cells) of full-length TMEM72 and 65 images (total 846 cells) of Δ132-137. Thirty-six images (total 407 cells) of Δ139-144 were used. The images involved in the quantitation were accessed from three independent immunofluorescence experiments. D. HeLa cells were transiently transfected with vectors for the expression of Δ132-137 and Δ139-144, as shown in Fig. 9A. Forty-eight hours after transfection, the cells were harvested and fractionated as described previously. Western blotting was performed to evaluate FLAG, cytoplasmic and nuclear ATF4, nuclear ATF4, phosphorylated eIF2α, and total eIF2α expression levels. Data are representative of three experiments. E-G. Quantification of three independent WB analyses as in Fig. 9D. H. Both spliced and total XBP1 mRNAswere quantified by qRT–PCR. Relative values for spliced/total XBP1 mRNA (%) were normalized to the control (mock). The data are presented as the means ± S.Ds.

Fig. 10. Essential roles of both KRKKRK and APEVLA ER export signal peptides in anterograde transport. A. HeLa cells were transiently transfected with vectors for the expression of Δ132-137 and Sec23A. At 24 h posttransfection, the

cells were coimmunostained using anti-FLAG (red) and Sec23A (green) antibodies. Scale bar = 20 μm. C. HeLa cells were transiently cotransfected with vectors for the expression of Δ139-144 and Sec23A. At 36 h posttransfection, the cells were coimmunostained using anti-FLAG (red) and Sec23A (green) antibodies. Scale bar = 20 μm. B, D. Quantification of Δ132-137 or Δ139-144 colocalization with Sec23A from three independent experiments. Each value represents Manders' overlap coefficient (fraction of the total fluorescence signal of Sec23A overlapping with the TMEM signal) obtained from confocal images. E. HeLa cells were transiently cotransfected with vectors for the expression of Δ132-137, TMEM72 and Sec23A. Twenty-four hours after transfection, the cells were subjected to immunoprecipitation with anti-FLAG beads. The whole-cell lysates and pulled-down samples were analyzed by western blotting using anti-FLAG and anti-Myc antibodies. F. Quantification of the protein level of Sec23A/IP FLAG by Co-IP. Three independent experiments were performed. G. HeLa cells were transiently cotransfected with vectors for the expression of TMEM72, Δ139-144, and Sec23A. At 36 h posttransfection, the cells were subjected to immunoprecipitation with anti-FLAG beads. The whole-cell lysates and pulled-down samples were analyzed by western blotting using anti-FLAG and anti-Myc antibodies. H. Quantification of the protein level of Co-IP Sec23A/IP FLAG normalized to TMEM72. The values were normalized to TMEM72, are expressed as the means ±S.Ds. and were statistically compared with TMEM72 via Student's ttest. Three independent experiments were performed. n.s.: not statistically significant.

Fig. 1

A

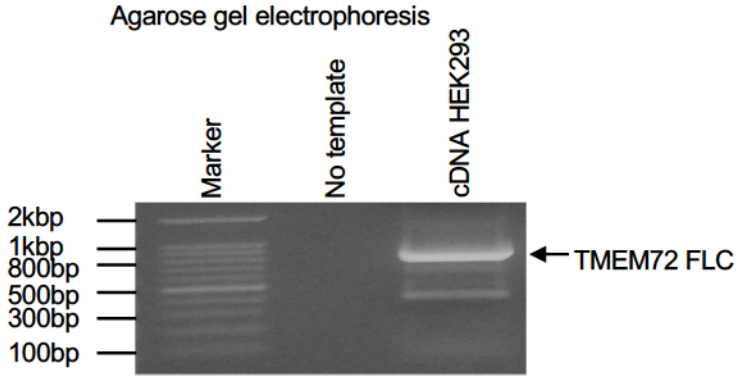
Agarose gel electrophoresis
Marker
No template
cDNA HEK293
2kbp
1kbp
800bp
500bp
300bp
100bp
TMEM72 FLC

B

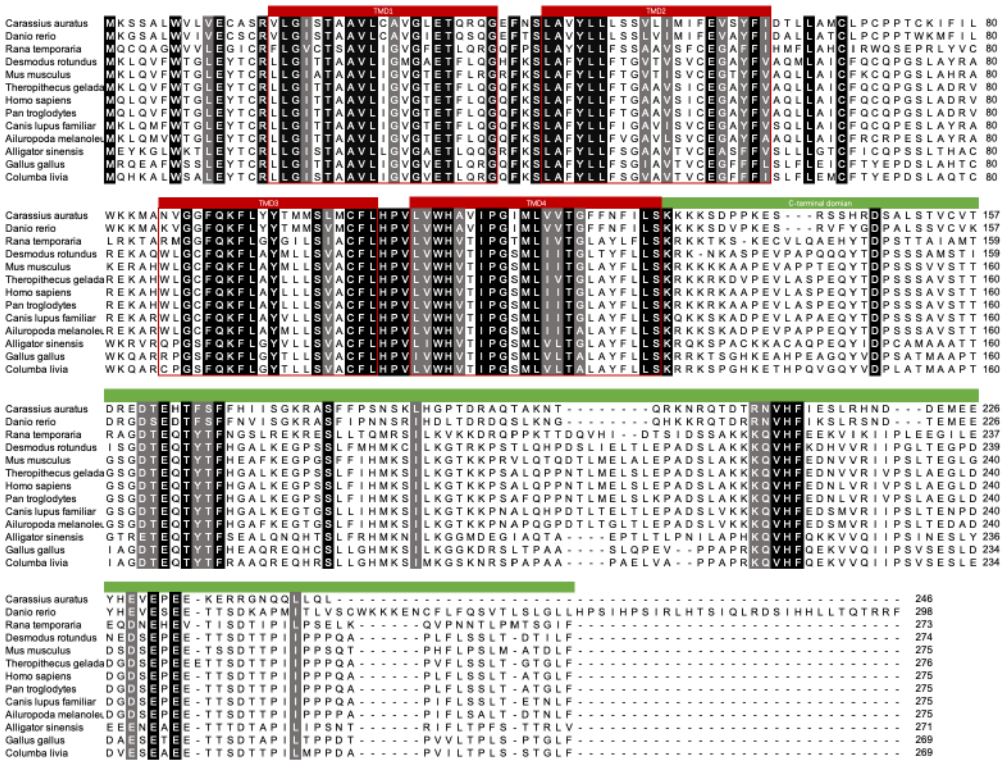
TM01
TM02
TM03
TM04
C-terminal domain
Carassius auratus
Danio rerio
Rana temporaria
Desmodus rotundus
Mus musculus
Theropithecus gelada
Homo sapiens
Pan troglodytes
Canis lupus familiar
Ailuropoda melanole
Alligator sinensis
Gallus gallus
Columba livia

Fig. 2

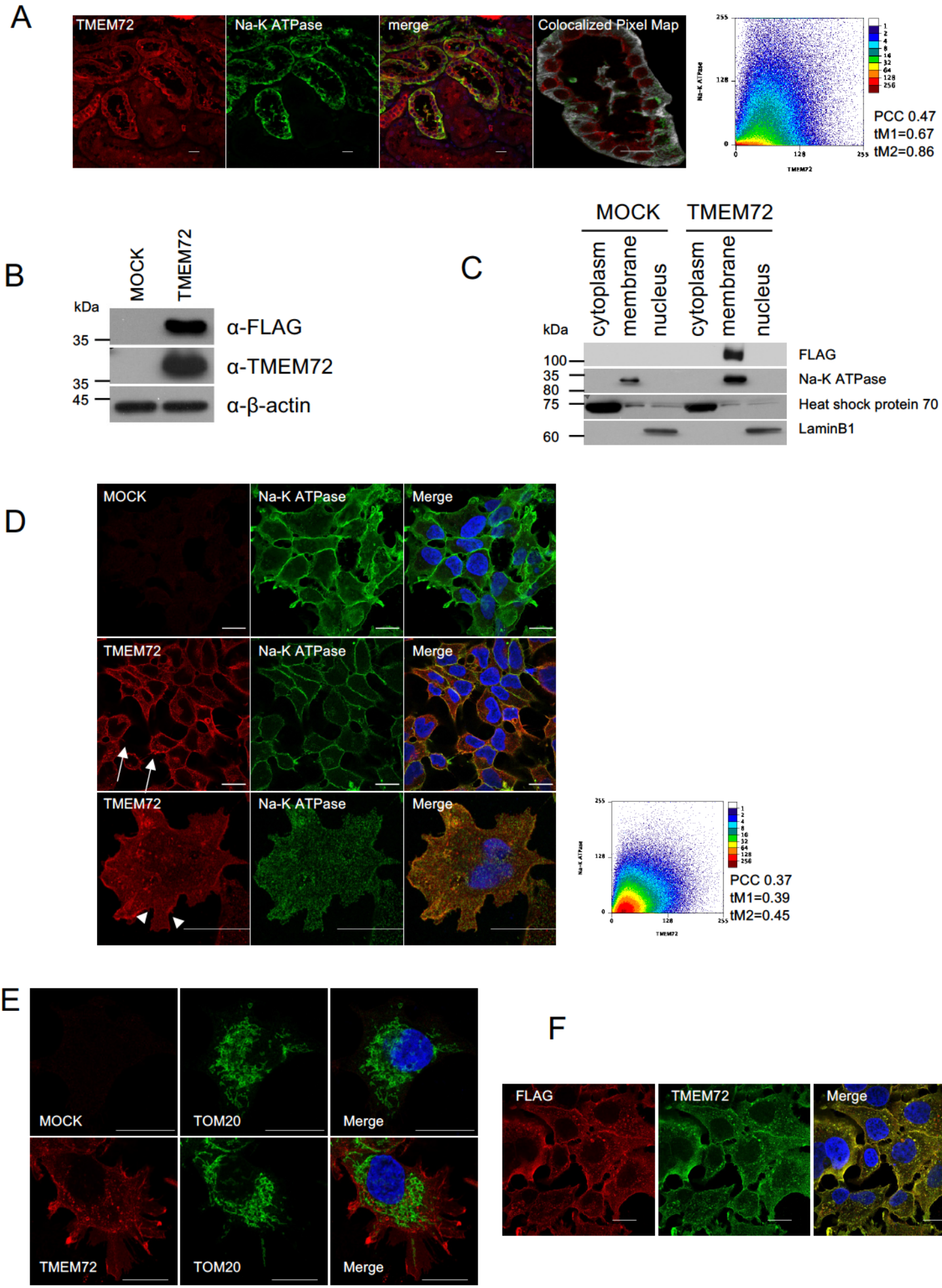
A
TMEM72
Na-K ATPase
merge
Colocalized Pixel Map
PCC 0.47
tM1=0.67
tM2=0.86
B
MOCK
TMEM72
kDa
35
35
45
α-FLAG
α-TMEM72
α-β-actin
C
MOCK
TMEM72
cytoplasm
membrane
nucleus
cytoplasm
membrane
nucleus
kDa
100
35
80
75
60
FLAG
Na-K ATPase
Heat shock protein 70
LaminB1
D
MOCK
Na-K ATPase
Merge
TMEM72
Na-K ATPase
Merge
TMEM72
Na-K ATPase
Merge
PCC 0.37
tM1=0.39
tM2=0.45
E
MOCK
TOM20
Merge
TMEM72
TOM20
Merge
F
FLAG
TMEM72
Merge

Fig. 3

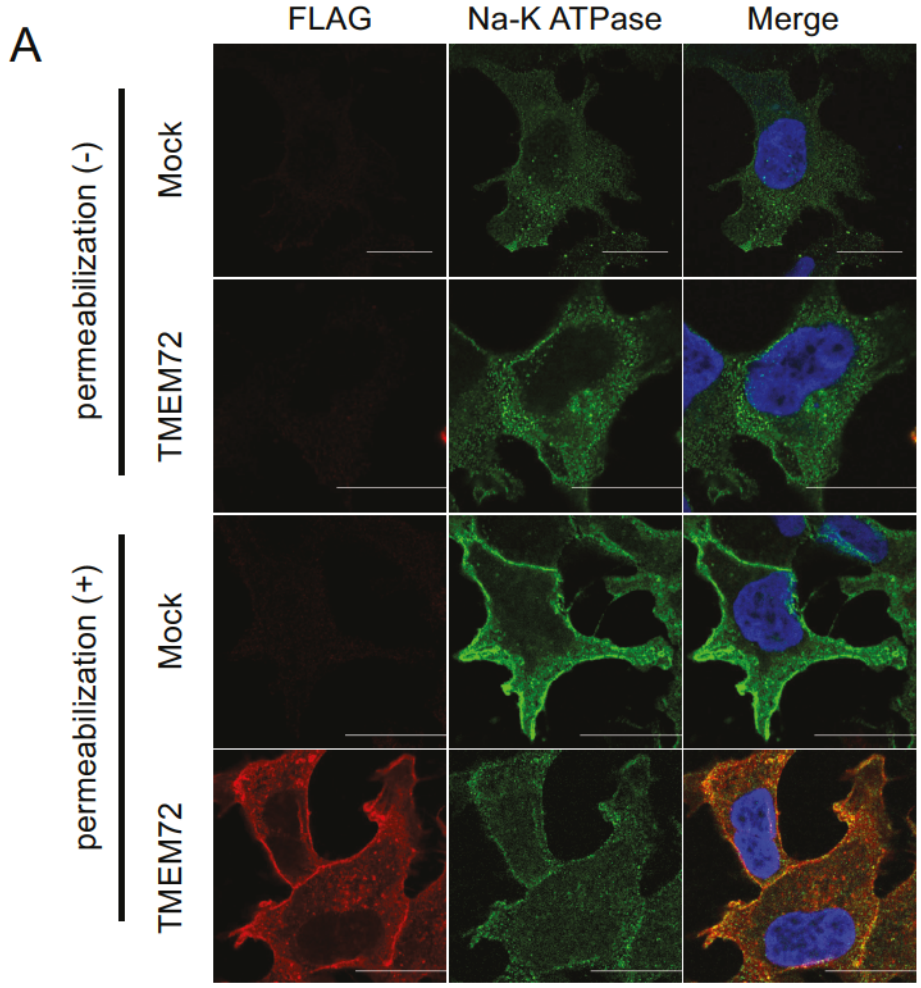
A
FLAG
Na-K ATPase
Merge
permeabilization (-)
Mock
TMEM72
permeabilization (+)
Mock
TMEM72

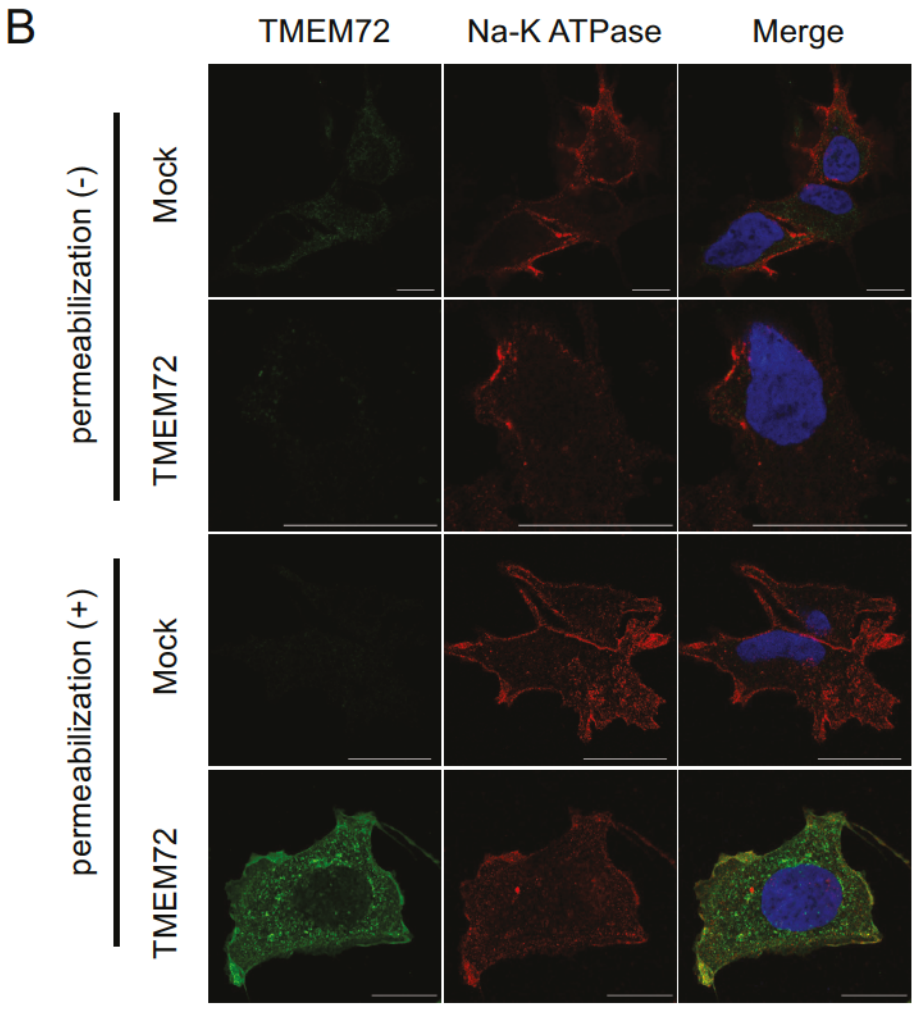
B
TMEM72
Na-K ATPase
Merge
permeabilization (-)
Mock
TMEM72
permeabilization (+)
Mock
TMEM72

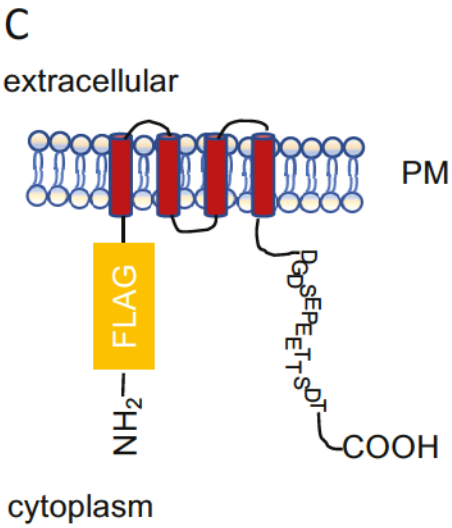
C
extracellular
PM
FLAG
NH2
COOH
cytoplasm

Fig. 4

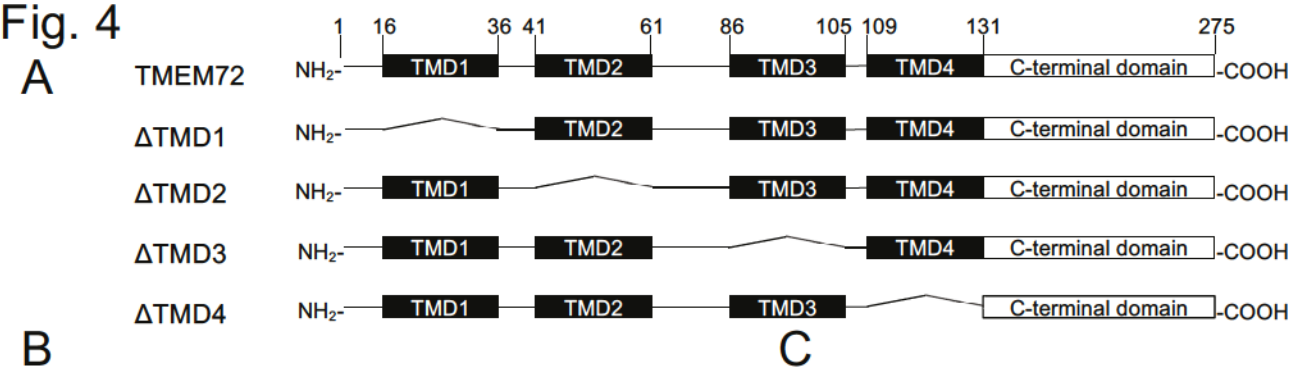
A
TMEM72
ΔTMD1
ΔTMD2
ΔTMD3
ΔTMD4
NH2-
TMD1
TMD2
TMD3
TMD4
C-terminal domain
-COOH
1
16
36
41
61
86
105
109
131
275

B C

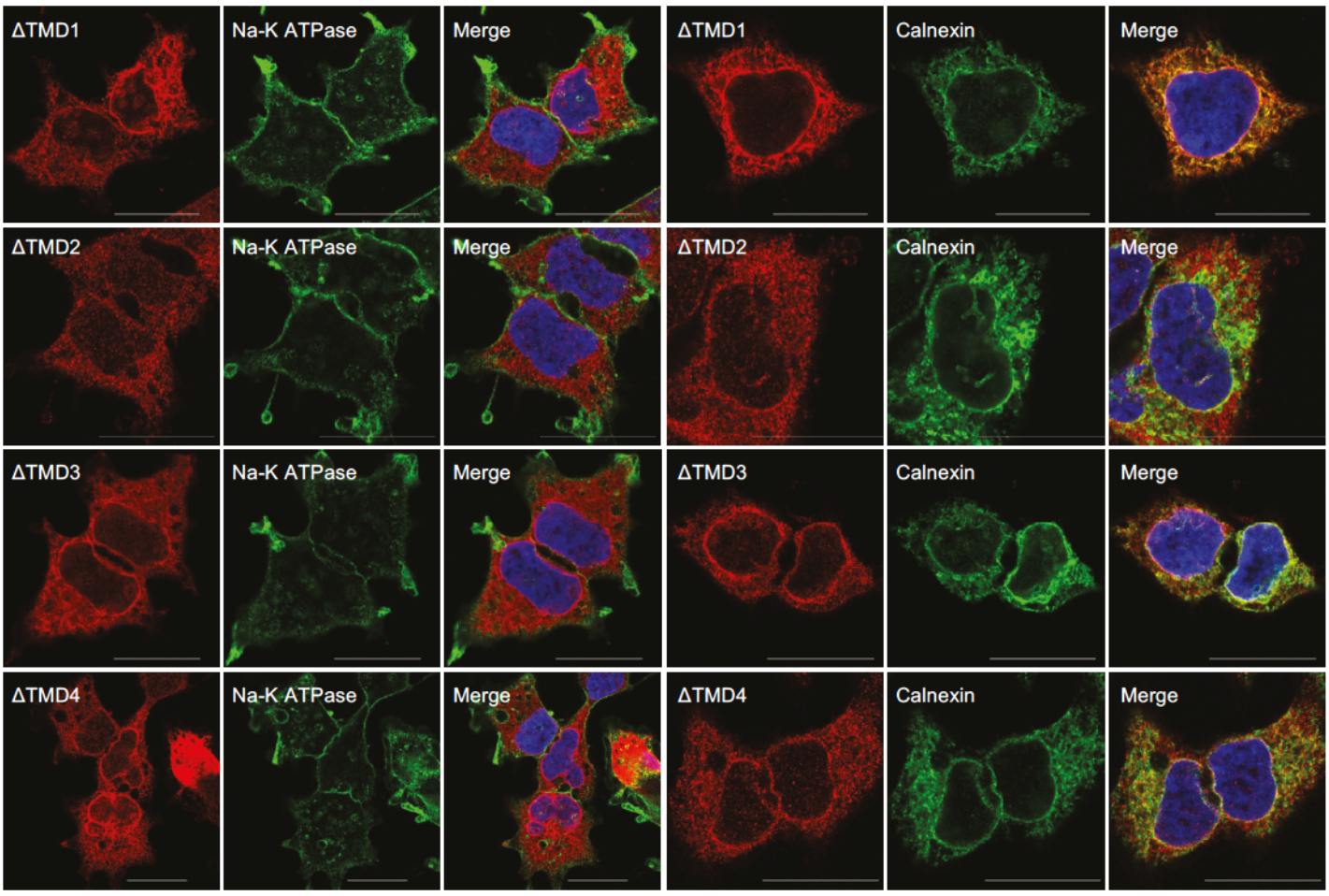
ΔTMD1
Na-K ATPase
Merge
ΔTMD1
Calnexin
Merge
ΔTMD2
Na-K ATPase
Merge
ΔTMD2
Calnexin
Merge
ΔTMD3
Na-K ATPase
Merge
ΔTMD3
Calnexin
Merge
ΔTMD4
Na-K ATPase
Merge
ΔTMD4
Calnexin
Merge

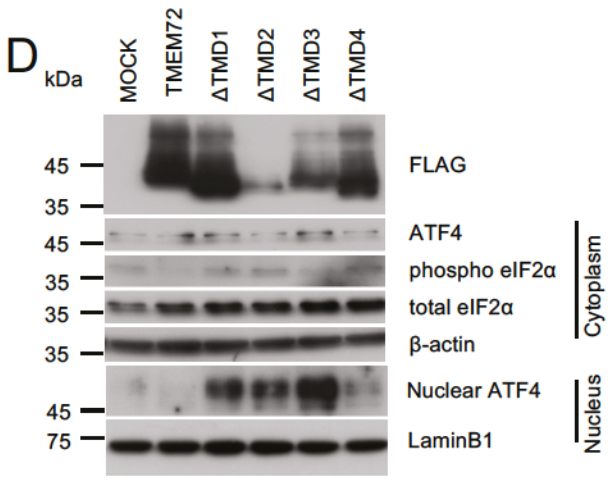
D
kDa
MOCK
TMEM72
ΔTMD1
ΔTMD2
ΔTMD3
ΔTMD4
45
35
45
35
35
35
45
75
FLAG
ATF4
phospho eIF2α
total eIF2α
β-actin
Nuclear ATF4
LaminB1
Cytoplasm
Nucleus

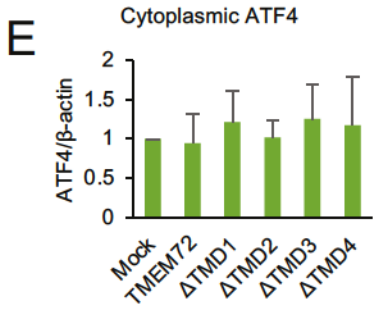
E
Cytoplasmic ATF4
ATF4/β-actin
2
1.5
1
0.5
0
Mock
TMEM72
ΔTMD1
ΔTMD2
ΔTMD3
ΔTMD4

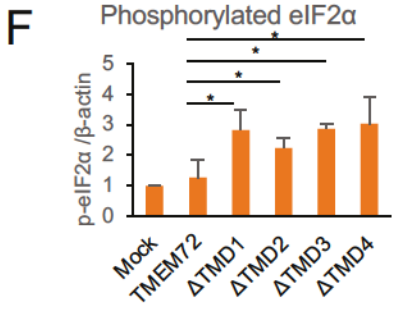
F
Phosphorylated eIF2α
p-eIF2α /β-actin
5
4
3
2
1
0
*
*
*
*
Mock
TMEM72
ΔTMD1
ΔTMD2
ΔTMD3
ΔTMD4

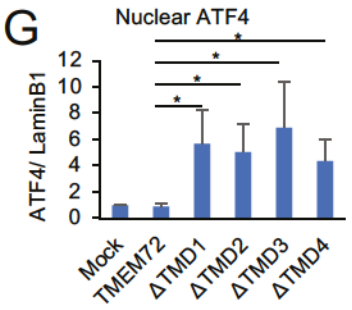
G
Nuclear ATF4
ATF4/ LaminB1
12
10
8
6
4
2
0
*
*
*
*
Mock
TMEM72
ΔTMD1
ΔTMD2
ΔTMD3
ΔTMD4

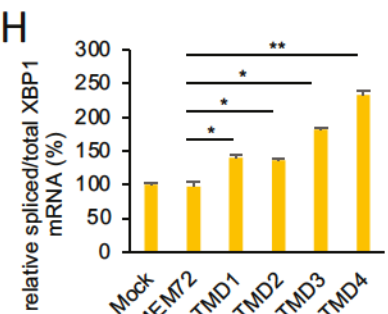
H
relative spliced/total XBP1 mRNA (%)
300
250
200
150
100
50
0
**
*
*
*
*
Mock
TMEM72
ΔTMD1
ΔTMD2
ΔTMD3
ΔTMD4

Fig. 5

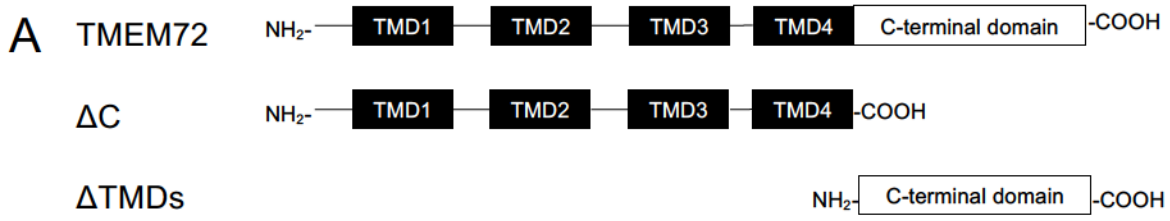
A
TMEM72
NH2-
TMD1
TMD2
TMD3
TMD4
C-terminal domain
-COOH
ΔC
NH2-
TMD1
TMD2
TMD3
TMD4
-COOH
ΔTMDs
NH2-
C-terminal domain
-COOH

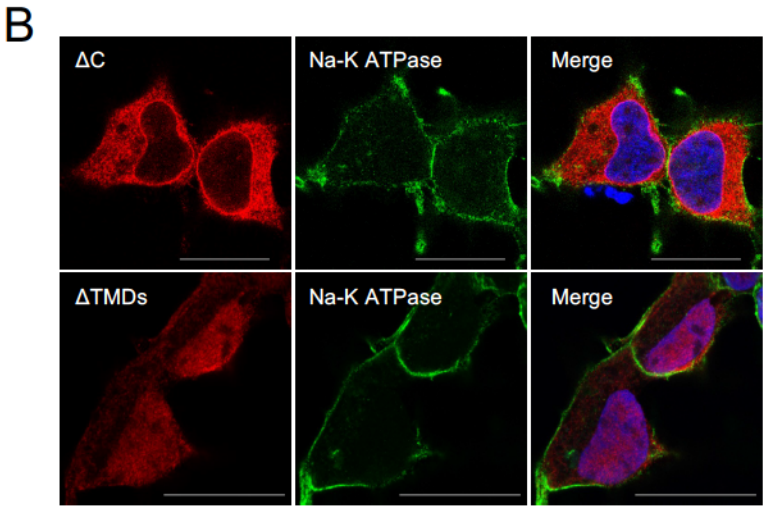
B
ΔC
Na-K ATPase
Merge
ΔTMDs
Na-K ATPase
Merge

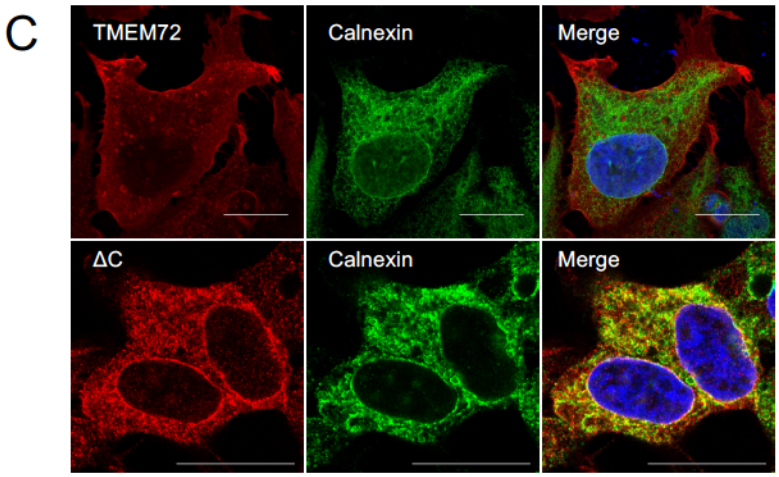
C
TMEM72
Calnexin
Merge
ΔC
Calnexin
Merge

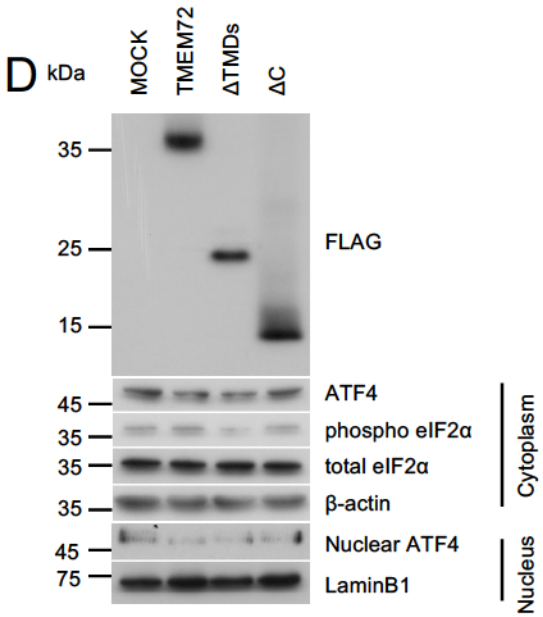
D
kDa
MOCK
TMEM72
ΔTMDs
ΔC
35
25
15
FLAG
45
35
35
35
ATF4
phospho eIF2α
total eIF2α
β-actin
Cytoplasm
45
75
Nuclear ATF4
LaminB1
Nucleus

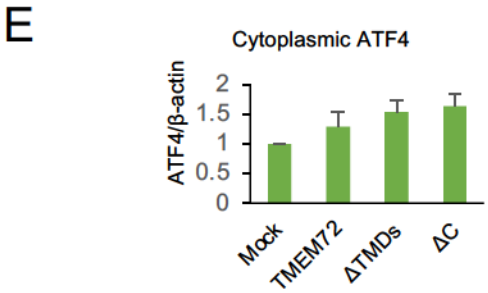
E
Cytoplasmic ATF4
ATF4/β-actin
2
1.5
1
0.5
0
Mock
TMEM72
ΔTMDs
ΔC

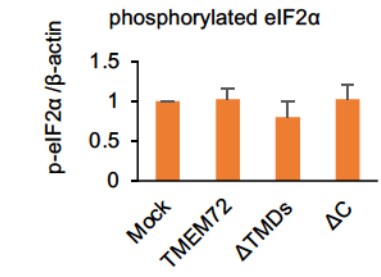
F
phosphorylated eIF2α
p-eIF2α /β-actin
1.5
1
0.5
0
Mock
TMEM72
ΔTMDs
ΔC

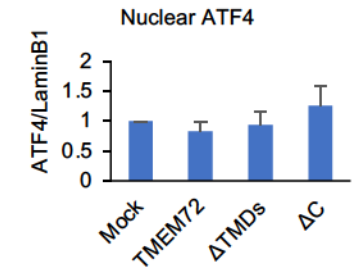
G
Nuclear ATF4
ATF4/LaminB1
2
1.5
1
0.5
0
Mock
TMEM72
ΔTMDs
ΔC

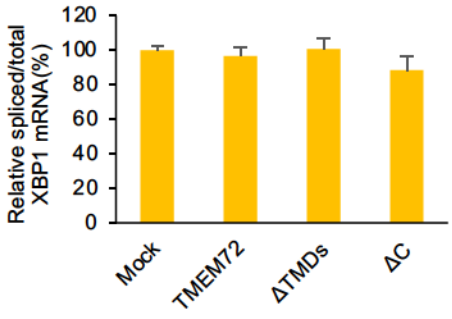
H
Relative spliced/total XBP1 mRNA(%)
120
100
80
60
40
20
0
Mock
TMEM72
ΔTMDs
ΔC

Fig.6

A

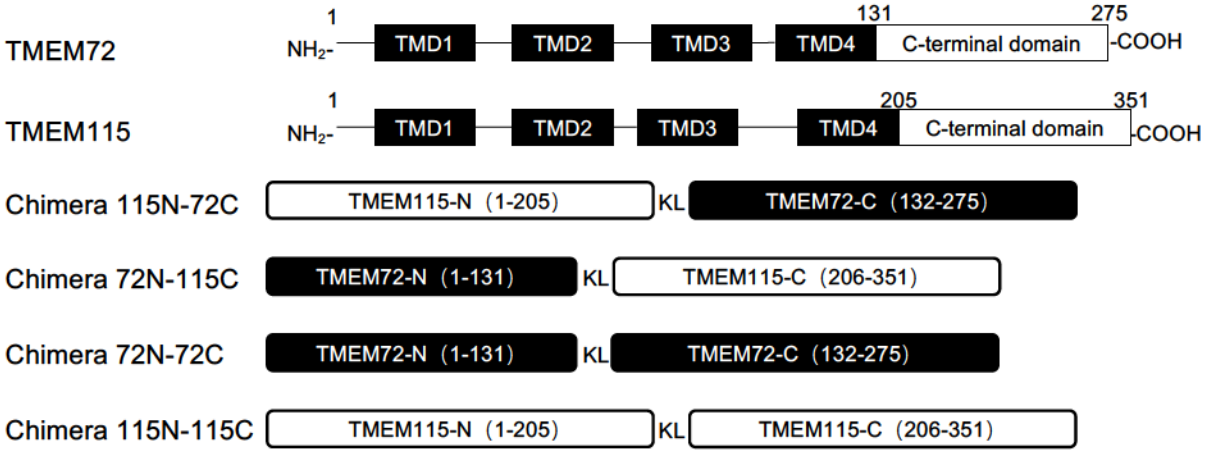

B

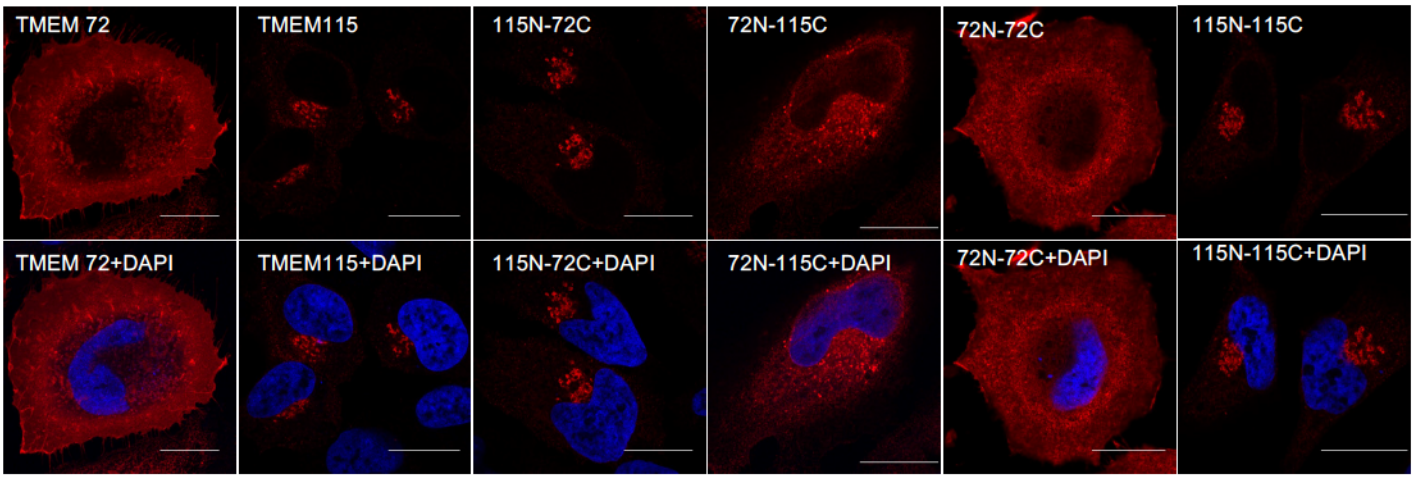

C

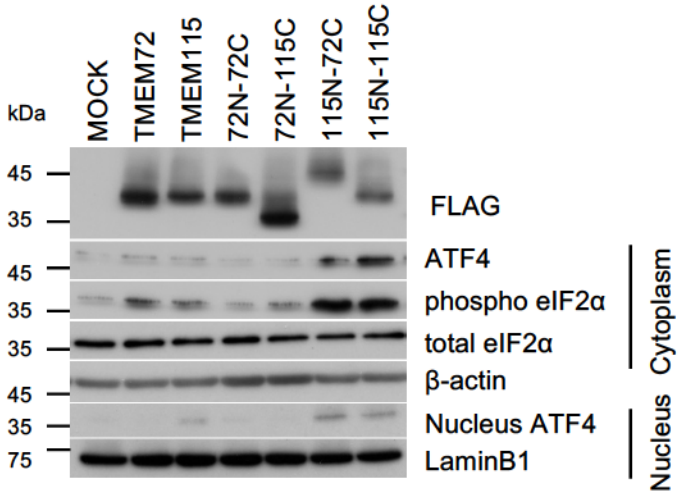

D

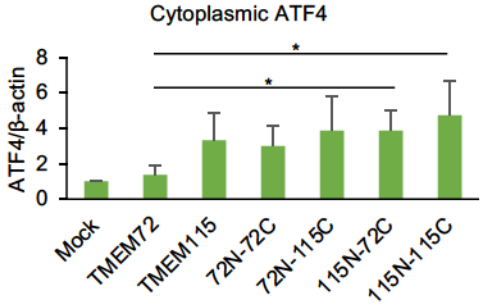

E

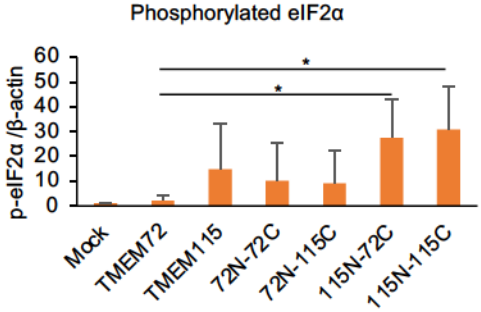

F

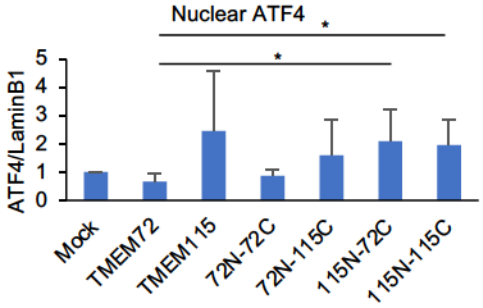

G

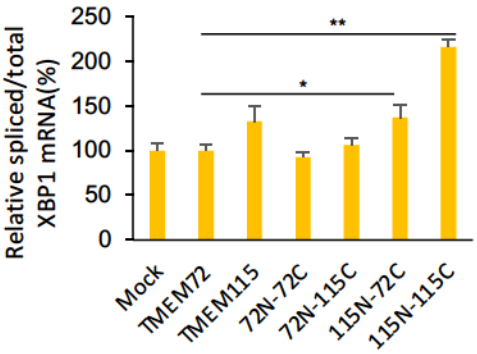

Fig. 7

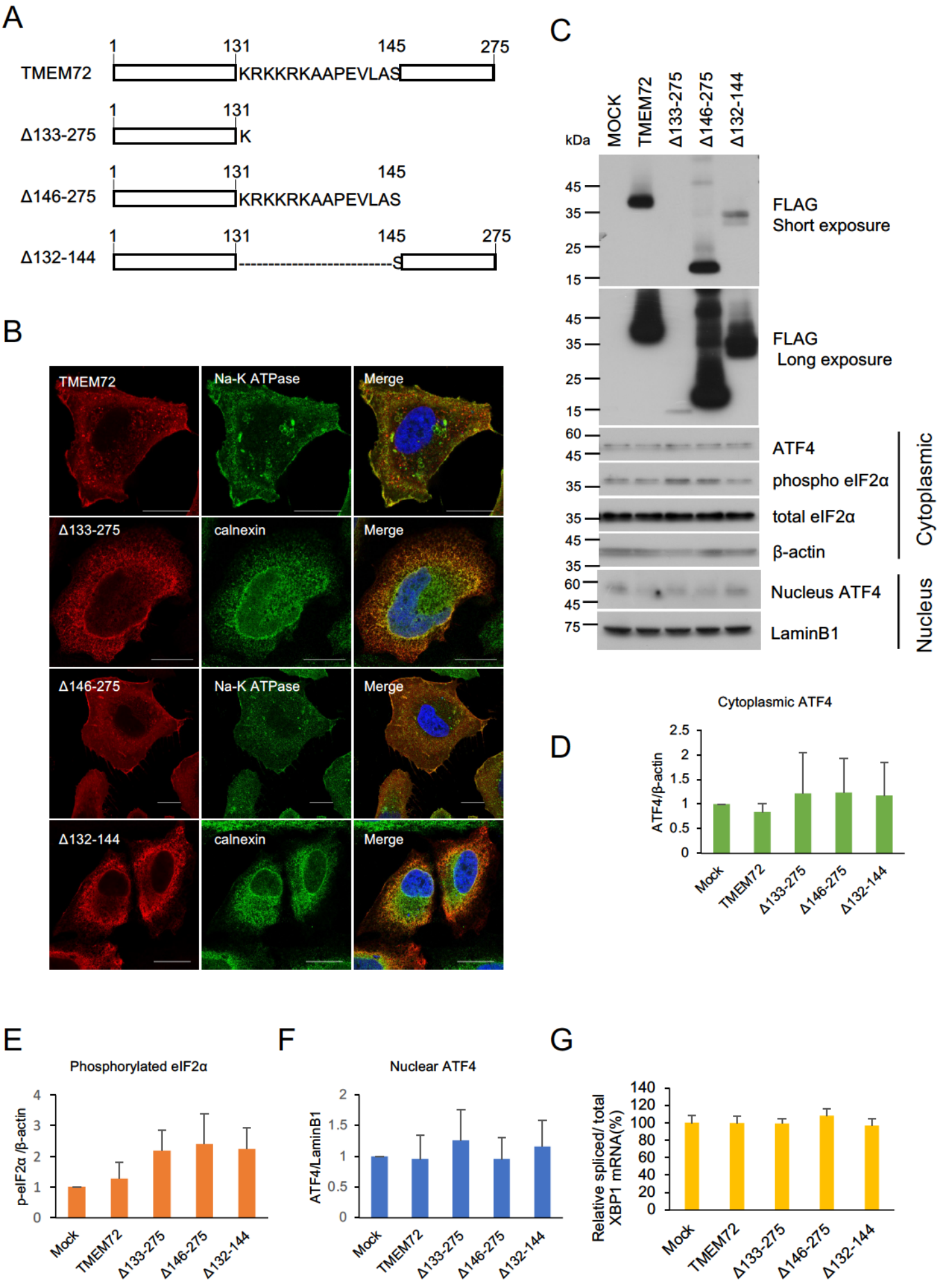
A
TMEM72
1
131
145
275
KRKKRKAAPEVLAS
Δ133-275
K
Δ146-275
KRKKRKAAPEVLAS
Δ132-144
S
B
TMEM72
Na-K ATPase
Merge
Δ133-275
calnexin
Merge
Δ146-275
Na-K ATPase
Merge
Δ132-144
calnexin
Merge
C
kDa
MOCK
TMEM72
Δ133-275
Δ146-275
Δ132-144
FLAG
Short exposure
FLAG
Long exposure
ATF4
phospho eIF2α
total eIF2α
β-actin
Cytoplasmic
Nucleus ATF4
LaminB1
Nucleus
D
Cytoplasmic ATF4
ATF4/β-actin
Mock
TMEM72
Δ133-275
Δ146-275
Δ132-144
E
Phosphorylated eIF2α
p-eIF2α /β-actin
F
Nuclear ATF4
ATF4/LaminB1
G
Relative spliced/ total XBP1 mRNA(%)

Fig. 8

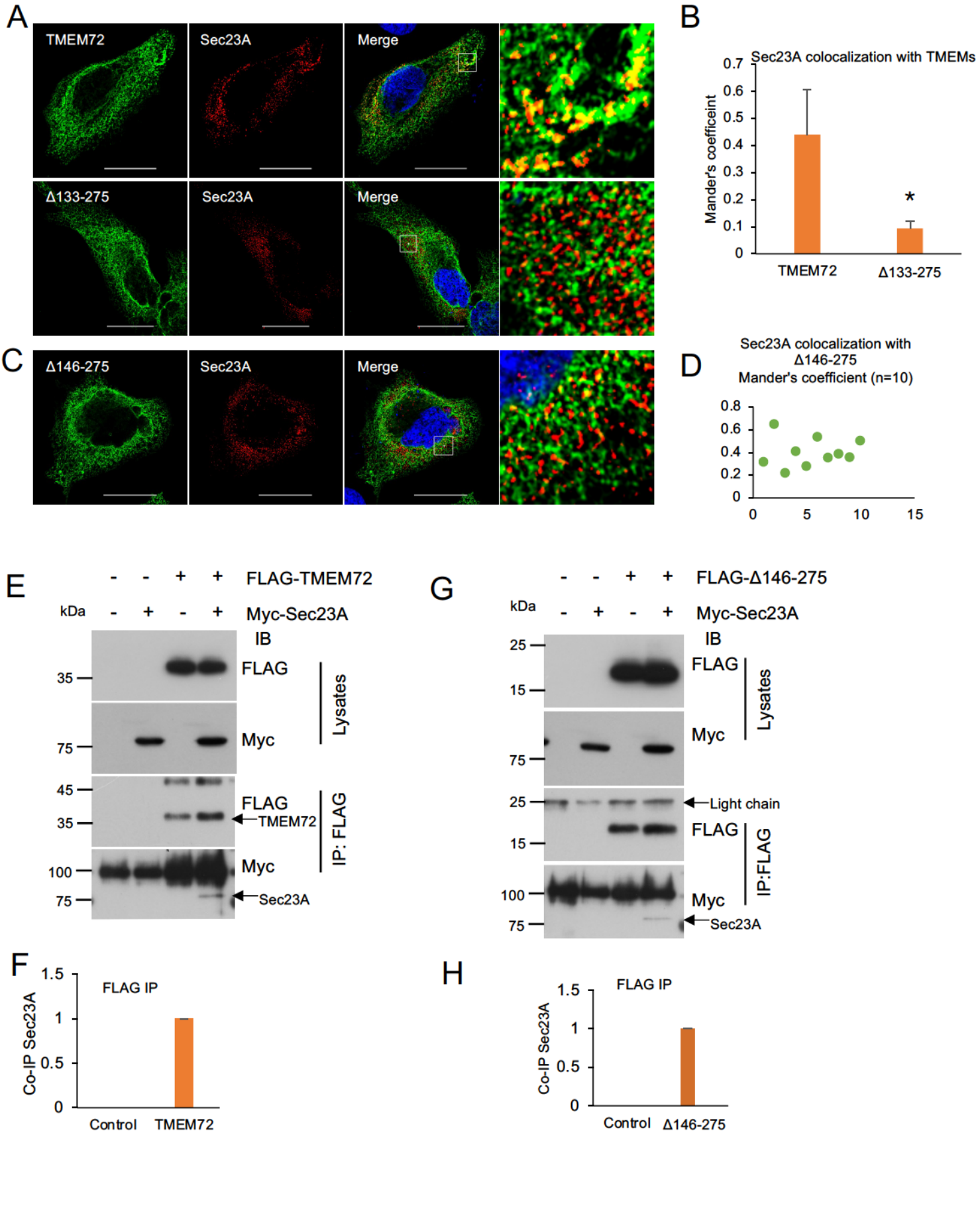
A
TMEM72
Sec23A
Merge
Δ133-275
Sec23A
Merge
C
Δ146-275
Sec23A
Merge
B
Sec23A colocalization with TMEMs
Mander's coefficeint
0.7
0.6
0.5
0.4
0.3
0.2
0.1
0
*
TMEM72
Δ133-275
D
Sec23A colocalization with
Δ146-275
Mander's coefficient (n=10)
0.8
0.6
0.4
0.2
0
0
5
10
15
E
FLAG-TMEM72
kDa
Myc-Sec23A
IB
35
FLAG
Lysates
75
Myc
45
35
FLAG
TMEM72
IP: FLAG
100
75
Myc
Sec23A
G
FLAG-Δ146-275
kDa
Myc-Sec23A
IB
25
15
FLAG
Lysates
75
Myc
25
Light chain
15
FLAG
IP:FLAG
100
75
Myc
Sec23A
F
FLAG IP
Co-IP Sec23A
1.5
1
0.5
0
Control
TMEM72
H
FLAG IP
Co-IP Sec23A
1.5
1
0.5
0
Control
Δ146-275

Fig. 9

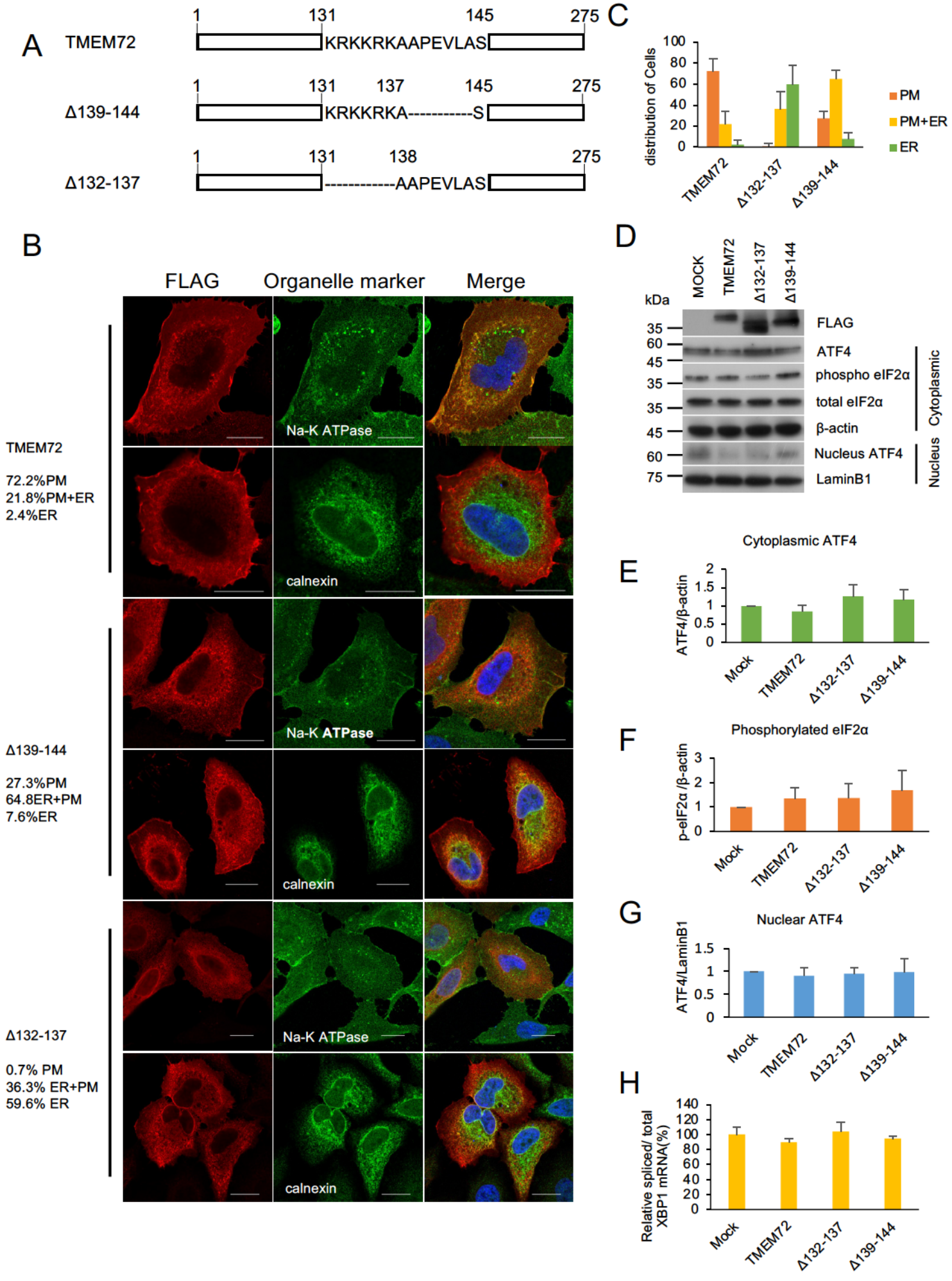
A
TMEM72
1
131
145
275
KRKKRKAAPEVLAS
Δ139-144
137
KRKKRKA----------S
Δ132-137
138
----------AAPEVLAS
B
FLAG
Organelle marker
Merge
Na-K ATPase
calnexin
TMEM72
72.2%PM
21.8%PM+ER
2.4%ER
Δ139-144
27.3%PM
64.8ER+PM
7.6%ER
Δ132-137
0.7% PM
36.3% ER+PM
59.6% ER
C
distribution of Cells
PM
PM+ER
ER
TMEM72
Δ132-137
Δ139-144
D
MOCK
TMEM72
Δ132-137
Δ139-144
kDa
FLAG
ATF4
phospho eIF2α
total eIF2α
β-actin
Nucleus ATF4
LaminB1
Cytoplasmic
Nucleus
E
Cytoplasmic ATF4
ATF4/β-actin
F
Phosphorylated eIF2α
p-eIF2α /β-actin
G
Nuclear ATF4
ATF4/LaminB1
H
Relative spliced/ total XBP1 mRNA(%)
Mock
TMEM72
Δ132-137
Δ139-144

Fig. 10

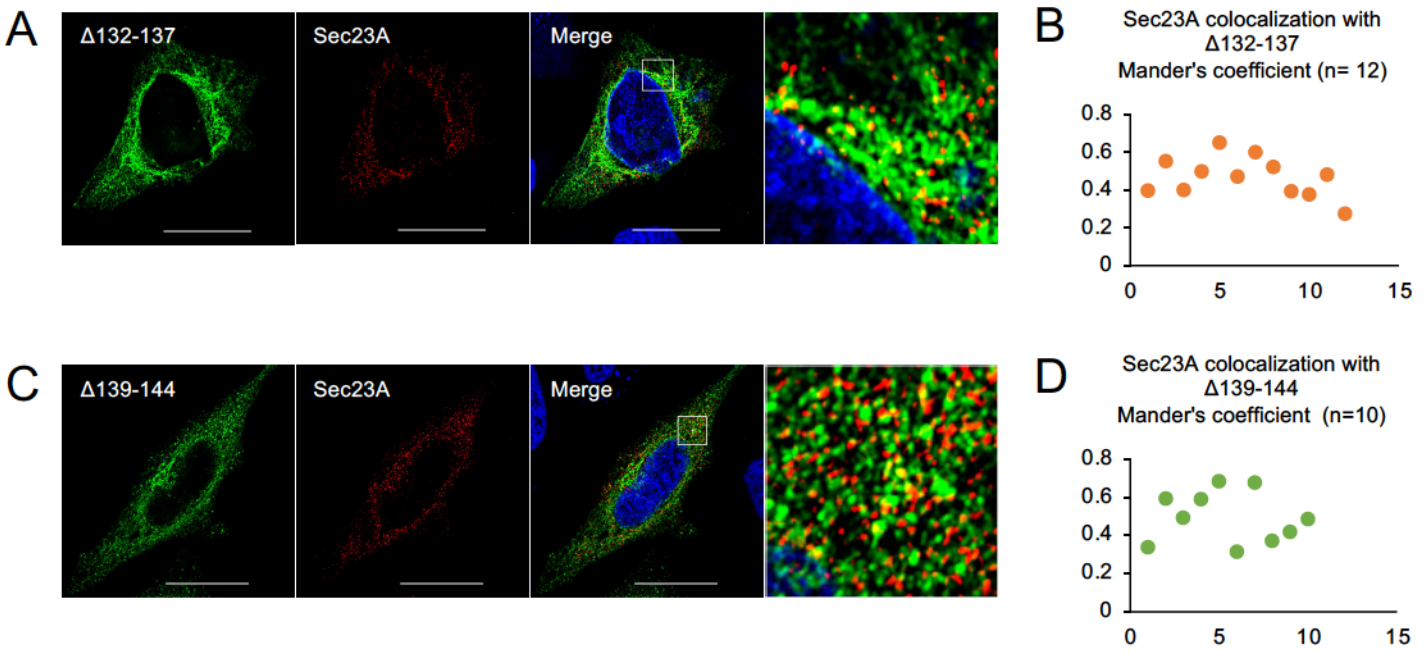
A
Δ132-137
Sec23A
Merge
B
Sec23A colocalization with
Δ132-137
Mander's coefficient (n= 12)
0.8
0.6
0.4
0.2
0
0
5
10
15
C
Δ139-144
Sec23A
Merge
D
Sec23A colocalization with
Δ139-144
Mander's coefficient (n=10)
0.8
0.6
0.4
0.2
0
0
5
10
15

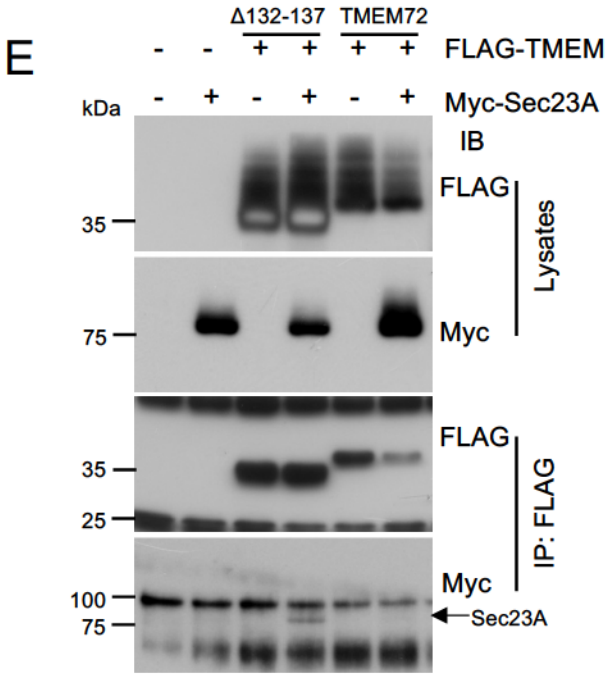
E
Δ132-137
TMEM72
- - + + + + FLAG-TMEM
kDa - + - + - + Myc-Sec23A
IB
35
FLAG
Lysates
75
Myc
35
25
FLAG
IP: FLAG
100
75
Myc
Sec23A

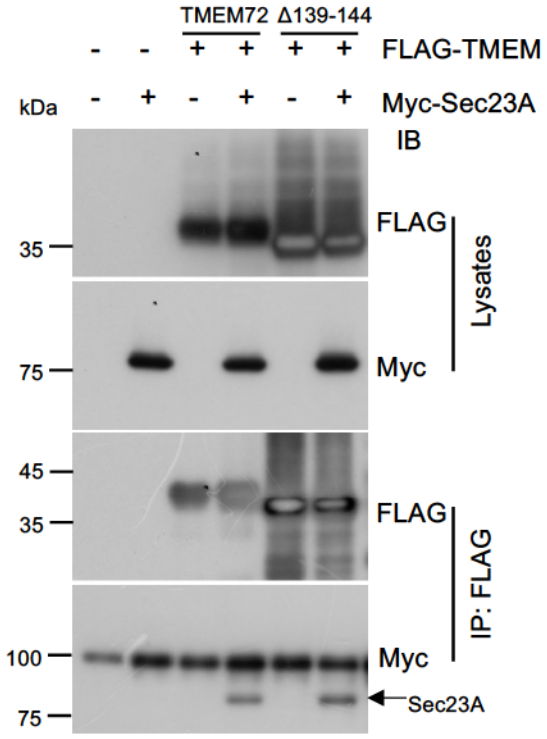
G
TMEM72 Δ139-144
- - + + + + FLAG-TMEM
kDa - + - + - + Myc-Sec23A
IB
35
FLAG
Lysates
75
Myc
45
35
FLAG
IP: FLAG
100
75
Myc
Sec23A

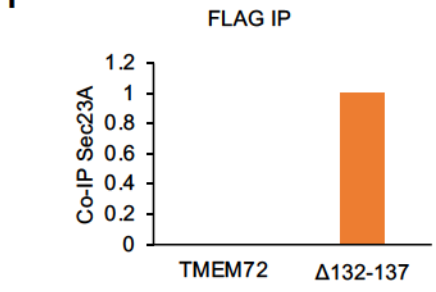
F
FLAG IP
Co-IP Sec23A
1.2
1
0.8
0.6
0.4
0.2
0
TMEM72
Δ132-137

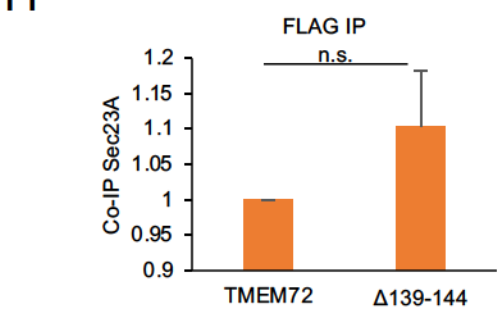
H
FLAG IP
n.s.
Co-IP Sec23A
1.2
1.15
1.1
1.05
1
0.95
0.9
TMEM72
Δ139-144